



Optimization of the number of elements for thermal maps utilizing Radtherm/RT  
by Allison Elizabeth Bristow

A thesis submitted in partial fulfillment of the requirements for the degree of Master of Science in  
Mechanical Engineering  
Montana State University  
© Copyright by Allison Elizabeth Bristow (2003)

Abstract:

In this thesis an analytical approach was used to optimize the number of elements required to produce accurate thermal maps utilizing RadTherm/RT. RadTherm/RT is a thermal model that uses all modes of heat transfer to predict road temperatures. The goal is to maximize the length of highway modeled and minimize the computation time. A methodology is implemented using a 4-part C/C++ algorithm to select particular elements to delete. The section of code that specifically determines the elements to delete is referred to as the view factor trim routine.

Initial steps are performed in order to obtain the information needed to determine the elements to delete. First, two files are necessary to create a new project in RadTherm/RT. Montana State University's Geographic Information and Analysis Center produced the ASCII files for elevation, road and vegetation maps using ARC/INFO GIS software. These files are loaded into RadTherm/RT to create a new project (.tdf). The project is executed to produce the view factor file (.vfs). Geometric view factors are used as the basis to eliminate elements. Radiation view factors are used in ThermoAnalytics' software to determine the intensity of radiation of each element to every other element in the model and to the environment. This allows the terrain model to include full effects of solar shadowing, multiple reflections, and reradiation of geometric objects. The geometric view factors of each element are calculated using ThermoAnalytics Ray Trace Algorithm and the results are stored in the view factor file (.vfs).

Two text files are required as input into the view factor trim routine. The first file contains the view factor information. This file is obtained by applying an algorithm written by ThermoAnalytics. The routine converts the view factor file (.vfs), which is in HDF format, to a text file. A second file is obtained by applying a routine that retrieves each element and its attributes, which includes the element number, part number, UTM coordinates, and elevation.

The view factor trim routine uses the element attributes and view factor information text files to determine which elements to delete from the model. The routine was developed to have the capability of designating any part(s) as the elements of interest, which are the elements of primary interest for temperature. Furthermore, the values used for the criteria to determine which elements to delete can be modified. The first criterion is the distance from the elements of interest, where all elements that meet this criterion are kept. The next criterion determines the minimum view factor value to keep an element that directly exchanges radiation with an element of interest. Similarly, a minimum view factor criterion is set for elements that emit to or receive energy from elements that have a direct radiation exchange to the elements of interest. The result from the view factor trim routine is a text file that contains the elements to delete.

The final part of the code uses the text file that contains the elements to delete and creates a new project in RadTherm/RT. The primary difference in the new project is that it contains a new part composed of the elements to delete. This allows a user to view the elements, before deleting them.

OPTIMIZATION OF THE NUMBER OF ELEMENTS FOR THERMAL MAPS  
UTILIZING RADTHERM/RT

by

Allison Elizabeth Bristow

A thesis submitted in partial fulfillment  
of the requirements for the degree

of

Master of Science

in

Mechanical Engineering

MONTANA STATE UNIVERSITY – BOZEMAN  
Bozeman, Montana

September 2003

© COPYRIGHT

by

Allison Elizabeth Bristow

2003

All Rights Reserved

N378  
B773

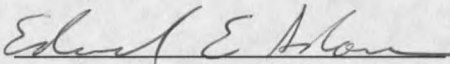
APPROVAL

of a thesis submitted by

Allison Elizabeth Bristow

This thesis has been read by each member of the thesis committee and has been found to be satisfactory regarding content, English usage, format, citations, bibliographic style, and consistency, and is ready for submission to the College of Graduate Studies.

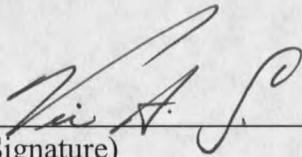
Dr. Edward E. Adams

  
(Signature)

3-SEPT-2003  
Date

Approved for the Department of Mechanical and Industrial  
Engineering

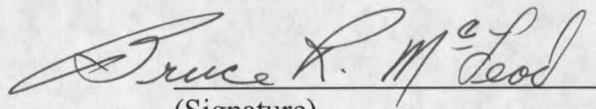
Dr. Vic A. Cundy

  
(Signature)

9/3/03  
Date

Approved for the College of Graduate Studies

Dr. Bruce R. McLeod


  
(Signature)

9-8-03  
Date

## STATEMENT OF PERMISSION TO USE

In presenting this thesis in partial fulfillment of the requirements for a master's degree at Montana State University – Bozeman, I agree that the library shall make it available to borrowers under rules of the Library.

If I have indicated my intention to copyright this thesis by including a copyright notice page, copying is allowable only for scholarly purposes, consistent with "fair use" as prescribed in the U.S. Copyright Law. Requests for permission for extended quotation from or reproduction of this thesis (paper) in whole or in parts may be granted only by the copyright holder.

Signature 

Date 9/2/03

## TABLE OF CONTENTS

1. CHAPTER 1 INTRODUCTION .....	1
2. CHAPTER 2 BACKGROUND .....	6
HEAT TRANSFER .....	6
Conduction .....	6
Convection .....	7
Radiation: Processes and Properties .....	7
Shortwave Radiation .....	9
Longwave Radiation .....	9
Radiation Exchange Between Surfaces .....	10
Surface Absorption, Reflection, and Transmission .....	10
Surface Emission .....	12
View Factor .....	12
RADTHERM/RT HEAT TRANSFER .....	23
Interior Layer Energy Balance .....	28
Surface Energy Balance .....	29
Energy Storage .....	30
Air Convection .....	30
Precipitation Convection .....	30
Ground Layer Conduction .....	31
Solar Load .....	31
Expanding Governing Equation .....	34
Net-radiation Method – Enclosure Theory .....	35
NUMERICAL METHOD OF SOLUTION .....	41
Transient Formulation .....	42
Computation of Temperature Distribution .....	44
3. CHAPTER 3 METHODOLOGY .....	46
RAY-TRACING ALGORITHM .....	46
View Factor Rays .....	49
View Factor Subdivisions .....	50
Apparent Area Resolution .....	50
Hand Calculation for View Factor .....	51
THE PROCESS TO DELETE ELEMENTS .....	52
Initial Setup .....	54
Step 1a - Digital Elevation Map Files (.asc) .....	54
Step 1b - Terrain File (.asc) .....	55
Step 2 - Trimming the Original Map .....	58

## TABLE OF CONTENTS - CONTINUED

Step 3 - RadTherm/RT Project Files (.tdf).....	60
Step 4 - Element Attribute File .....	63
Step 5 - View Factor File (.vfs) .....	65
Step 6 – Code to Delete Elements.....	68
Step 6a – Separate Elements.....	69
Step 6b – Apply Distance Criteria .....	70
Step 6c – View Factors to Elements of Interest.....	71
Step 6d – View Factors to Elements with View Factors to Elements of Interest.....	73
Step 6e – Output File .....	75
Step 7 – Create a new part .....	76
Creating a RadTherm Project.....	76
4. CHAPTER 4 FINDINGS/RESULTS .....	80
RADIATION EXCHANGE – SIMPLE MODEL .....	80
Shadowing Effects .....	81
Shortwave Radiation Exchange .....	84
180° Flat Model.....	85
135° Model.....	87
90° Model.....	92
Longwave Radiation Exchange .....	98
MODEL OF BOZEMAN PASS .....	104
No View Factor or Distance Criteria .....	111
No View Factor and Distance Criteria Set.....	113
View Factor and Distance Criteria Set.....	115
Evaluate View Factor Criterion .....	115
Results.....	118
MODEL OF ROCKY CANYON .....	120
Coordinates for Rocky Canyon Model .....	120
Assign RadTherm/RT Part ID. ....	123
Location for Temperature Comparison.....	127
Summer Test Case – July 2 <sup>nd</sup> , 2003 .....	129
Weather File - Summer.....	129
Temperature Comparison – Mile Marker 315 .....	131
Temperature Comparison – Mile Marker 315½ .....	132
Temperature Comparison – Mile Marker 316 .....	132
Temperature Comparison – Mile Marker 316½ .....	133
Temperature Comparison – Mile Marker 317 .....	133
Temperature Comparison – Mile Marker 317½ .....	135

## TABLE OF CONTENTS - CONTINUED

Temperature Comparison – Mile Marker 318 .....	135
Winter Test Case – February 2 <sup>nd</sup> , 2003.....	136
Weather File - Winter .....	136
Temperature Comparison – Mile Marker 315 .....	137
Temperature Comparison – Mile Marker 315½ .....	137
Temperature Comparison – Mile Marker 316 .....	140
Temperature Comparison – Mile Marker 316½ .....	140
Temperature Comparison – Mile Marker 317 .....	141
Temperature Comparison – Mile Marker 317½ .....	142
Temperature Comparison – Mile Marker 318 .....	143
5. CHAPTER 5 SUMMARY/CONCLUSIONS.....	144
6. REFERENCES CITED.....	150
7. APPENDICES .....	152
APPENDIX A: C/C++ CODE – RETRIEVE ELEMENT ATTRIBUTES .....	153
APPENDIX B: C/C++ CODE – VIEW FACTOR TRIM ROUTINE .....	160
APPENDIX C: C/C++ CODE – UPDATE RADTHERM PROJECT FILE .....	179

## LIST OF TABLES

Table	Page
1. View factor ray setting in RadTherm/RT. ....	50
2. View factor ray setting in RadTherm/RT. ....	52
3. Land cover classification system used by Montana Gap Analysis Project.....	56
4. Summary of the iterations for trimming a map of Bozeman Pass to a size that produces the view factor file (.vfs). ....	59
5. Solar Azimuth and Zenith angles at two-hour increments on July 22, 1993.....	83
6. (a) View factor values for Figure 48a. Receiver #17 is the sky node. (b) View factor values for Figure 48b. Receiver #26 is the sky node.....	87
7. The absorptivity values for the sloped terrain for each case.....	88
8. View factors for Element 10 labeled on Figure 50b with $\theta = 135^\circ$ . (a) Shows the receiving elements that element 10 emits to. Note that receiver number 26 is the sky node. (b) The elements that emit to element 10. ....	89
9. View factors for Element 10 labeled for a rock wall at $135^\circ$ , and for a rock wall at $90^\circ$ . ....	93
10. The percentage of the view factor values for element 40 in each model in Figure 60. ....	100
11. Results for the model of Bozeman Pass with the distance criterion and view factor criteria set to zero. For this case, 82,075 elements were deleted.....	112
12. Results for the model of Bozeman Pass with the distance criterion set to 250-meters and the view factor criteria set to zero. For this case, 81,448 elements are deleted. ....	113
13. The emissivity values for the terrain types in RadTherm/RT.....	116

## LIST OF TABLES - CONTINUED

Table	Page
14. Results for the model of Bozeman Pass with the distance criterion set to 250-meters and the view factor criteria set to 0.0005. For this case, 288,308 elements are deleted. ....	118
15. Results for Rocky Canyon using the view factor trim routine with the distance criteria set to 0 and the view factor criteria set to 0.0005. ....	123
16. Land cover classifications mapped to RadTherm/RT part ID's. ....	125
17. Each RadTherm/RT part and the associated properties. ....	127
18. The temperatures are compared at each ½ mile between mile marker 315 and 318. The UTM coordinates and element numbers at listed for each location. ....	128

## LIST OF FIGURES

Figure	Page
1. Electromagnetic Spectrum (After Incropera and DeWitt, 1996, Figure 12.3).....	8
2. Absorbed, reflected, and transmitted shortwave radiation with a semitransparent medium. ....	11
3. Radiation emitted by a surface. (a) Spectral distribution. (b) Directional distribution. (After Incropera and DeWitt, 1996, Figure 12.4).....	13
4. Radiation emitted from a point in differential area $dA_1$ into a solid angle $d\omega$ subtended by differential area $dA_n$ . (After Incropera and DeWitt, 1996, Figure 12.5).....	14
5. (a) Definition of a plane angle. (b) Definition of a solid angle. (After Incropera and DeWitt, 1996, Figure 12.6).....	15
6. In the spherical coordinate system, a solid angle subtended by $dA_n$ from a point on $dA_1$ . (After Incropera and DeWitt, 1996, Figure 12.7).....	16
7. Two surface normals of the differential areas $dA_i$ and $dA_j$ . $\theta_i$ and $\theta_j$ are the angles to the line connecting the two bodies. ....	17
8. The projection of $dA_i$ and $dA_j$ normal to the direction of radiation. ....	17
9. The differential solid angle subtended by $dA_j$ from a point on $dA_i$ . ....	18
10. A diffuse reflector. ....	20
11. Surface radiosity. ....	21
12. A mesh created for RadTherm/RT for a region of interest. ....	24
13. A single soil element and the associated layers. ....	25
14. Heat transfer modes for each node. ....	26
15. Angle of incidence. ....	33

## LIST OF FIGURES - CONTINUED

Figure	Page
16. Energy quantities incident upon and leaving a typical surface of an enclosure .....	37
17. The position of the sun is specified in terms of the zenith and azimuth angles, $\theta$ and $\phi$ , respectively.....	48
18. (a) A single ray cast from an element for ThermoAnalytics Ray Trace Algorithm. (b) Multiple rays cast from an element for ThermoAnalytics Ray Trace Algorithm. (Figures from ThermoAnalytics, Inc. website).....	49
19. (a) A simple model used for the hand calculation of the view factor. The model consists of two finite rectangles of the same length, having one common edge at an angle of $90^\circ$ to each other. (b) The equation used to calculate the view factor from 1 to 2. (After Siegel and Howell, Figure 16 in the Appendix) .....	51
20. Example of ASCII input file for elevation data created from USGS 30 meter grid.....	55
21. Example of the ASCII input file for the terrain and road information. This file has been converted from the land classification to RadTherm/RT Part ID's. Note that 1 represents a part ID such as the road.....	57
22. Command line to execute the gis_manip PERL script. ....	59
23. (a) Set each part to type terrain. (b) Specify a weather file. (c) Set the same start and end solution times.....	61
24. Flow chart of Steps 1 through 3. Step 1 is generating the ASCII files. Step 2 determines the UTM coordinates for a map with less than 330,000 elements. Step 3 creates a new project in RadTherm/RT. ....	62
25. Example of a RadTherm/RT project composed of 2 parts. ....	63
26. Step 4 of the procedure. A C/C++ code is used to create a text file with the element attributes: Element ID, Part ID, UTM coordinates, and elevation.....	64
27. Example of the text file that contains the element attributes. This is the output file from Step 4. ....	65

## LIST OF FIGURES - CONTINUED

Figure	Page
28. Flow chart for Step 5. This step converts the view factor file to an ASCII text file.....	66
29. The command line to execute the vf2asc utility .....	66
30. This is the output file from Step 5. Example of the view factor file produced from the vf2asc executable. ....	67
31. Flow chart for an overview of Step 6. The Element Attribute text file and View factor text file are used as input into Step 6. The output from Step 6 is a text file containing the elements to delete. ....	68
32. Flow chart for Step 6a. This step separates all the surface elements for the terrain map into two categories. The first category is the elements of interest with a rank of 1 and the second category is the surrounding elements with a rank of 2. ....	69
33. A simple demonstration terrain model to describe the ranking after Step 6a. ....	70
34. Simple demonstration terrain model to describe the ranking after Step 6b. ....	71
35. Illustrates the three options for Step 6c. The emitter is an element of interest, or the receiver is an element of interest, or neither the emitter nor receiver is an element of interest. ....	72
36. Simple demonstration terrain model to describe the ranking after Step 6c. ....	73
37. Simple demonstration terrain model to describe the ranking after Step 6d. ....	74
38. Summary of the ranks applied to the elements in Steps 6a, 6b, 6c, and 6d. ....	75
39. An example of the output text file from Step 6e. The first row of the file contains the number of elements to delete. The subsequent rows are the element numbers to delete (R = 1). ....	76
40. Summary of steps 6b through 6e. ....	77

## LIST OF FIGURES - CONTINUED

Figure	Page
41. Flow chart for Step 7. The elements to delete, which are contained in the text file, are assigned to a new Part ID. ....	78
42. Example of the new update.tdf project created for RadTherm/RT. A new part has been created (Part 18) labeled "Elements to Delete". ....	79
43. Example of the update.tdf project after Part 18, which contains the elements to delete, has been removed.....	79
44. Simple model to demonstrate importance of shading. A represents the interstate and B represents a wall of rock. ....	81
45. A simple model that represents a flat highway.....	82
46. A temperature plot for element 6 of the interstate without a rock wall versus element 6 of the interstate with a rock wall. The plot is from 12:00 AM on July 22, 1993 to 12:00 PM on July 23, 1993. ....	83
47. The side view of a model with a sloped rock wall with a varying angle $\theta$ .....	84
48. (a) Simple model of the interstate with fifteen surface elements. (b) Simple model of the interstate with an adjoining terrain part composed of nine surface elements (16-24) and modeled as rock.....	85
49. Plot of the 24-hour temperature output for Element 10 for both models described in Figure 48b.....	86
50. (a) Side view of the model with the sloped wall at an angle of $135^\circ$ . (b) A model composed of two parts. Part A is the interstate with fifteen elements. Part B is the sloped wall at $135^\circ$ from the interstate.....	88
51. The temperature plot for Element number 10 for two cases. A rock slope with: 1) an absorptivity ( $\alpha$ ) of 0.05 and 2) $\alpha = 0.90$ .....	91
52. The temperature plot for Element number 20 for both cases. For the first case, the rock slope has an absorptivity ( $\alpha$ ) of 0.05 and in the second case, $\alpha = 0.90$ . Element 20 is the center element on the sloped terrain.....	92

## LIST OF FIGURES - CONTINUED

Figure	Page
53. (a) Side view of the simple model consisting of two parts, the interstate and a rock wall at and angle of 90°. (b) A simple RadTherm/RT model consisting of two parts, the interstate and a rock wall at 90°. Fifteen elements are assigned to the interstate and nine elements are assigned to the rock wall at 90°.	92
54. The temperature plot for Element 10 for both cases. For the first case, the rock slope has an absorptivity of 0.05 and in the second case has an absorptivity of 0.90.	94
55. The temperature plot for 90 degree wall, Element 20 for two cases. With a rock slope that has 1) an absorptivity ( $\alpha$ ) of 0.05 and 2) $\alpha = 0.90$ .	95
56. The highway temperature of Element 10 for the model with a sloped terrain at 135° and 90° with an absorptivity value of 0.90.	96
57. The temperature plot of Element 10 for the model with terrain sloped at 135° and 90° with an absorptivity value of 0.05.	97
58. Side view of the models used to compare the longwave radiation effects. (a) Simple model without a left rock wall. (b) Simple model with a rock wall on the left side.	98
59. The model used to compare the longwave radiation effects with the pertinent elements labeled.	100
60. The temperature plot of interstate element 40 for both models. Note that the solar radiation is set to zero at 9:50 AM.	101
61. The temperature plot of Element 40 where the left rock wall increases in 10-meter segments.	102
62. A plot of the temperature of interstate Element 40 to Element 112 on the left rock wall.	103
63. A plot of the temperature of interstate Element 40 (with no left wall) to the sky temperature for the model.	104

## LIST OF FIGURES - CONTINUED

Figure	Page
64. The UTM coordinates used to create the model for Bozeman Pass. ....	104
65. RadTherm/RT model for Bozeman Pass consisting of 327,610 surface elements and 17 parts.....	105
66. The Part ID that contains the elements of interest must be specified. The two lines of code that must be set for Step 6 are labeled A and B.....	107
67. A simple model to illustrate the distance criterion set at 100 meters. ....	108
68. The distance criterion in Step 6b is assigned in the code, which is labeled as C. In this case, the distance criterion is 250 meters.....	109
69. The view factor criteria must be set for lines D and E. In this case, the view factor criteria are 0.0005.....	109
70. This is the identical model as in Figure 65, but contains an additional part. This part (Part 18) contains the elements to delete. ....	110
71. A magnified picture of the interstate through Bozeman Pass. The empty spaces are a result of the deleted elements.....	112
72. The resulting model of Bozeman Pass with the distance criterion set to 250 meters and the view factor criteria set to zero. Only 82,000 surface elements have been deleted and 245,000 surface elements remain in the model.....	114
73. Plot of Equation (81), which is the energy lost or gained from surface element $k$ to $j$ . The x-axis is the radiation from surface element $j$ and varies from 0 to 50,000 Watts. The graph plots the radiation term of surface $k$ for four different temperature values of $j$ . ....	117
74. The resulting model of Bozeman Pass with the distance criterion set to 250 meters and the view factor criteria set to 0.0005. 288,308 surface elements have been deleted and 39,302 surface elements remain in the model.....	119

## LIST OF FIGURES - CONTINUED

Figure	Page
75. The region selected for the model of Rocky Canyon. The interstate spans from mile marker 314½ to mile marker 318.....	121
76. A 3-dimensional map of Interstate 90 through Rocky Canyon from mile marker 314 heading east. ....	121
77. RadTherm/RT model for Rocky Canyon consisting of 33,096 surface elements. ....	122
78. RadTherm/RT model for Rocky Canyon after the view factor trim routine is applied. The distance criterion was set at zero and the view factor criteria were set at 0.0005. This model consists of 5,777 surface elements.....	124
79. An example of the RadTherm/RT GUI for a foliage terrain part. ....	126
80. Meteorological Plots from 12:00 am on July 2 <sup>nd</sup> , 2003 for (a) air temperature vs. time (b) solar radiation vs. time (c) cloud cover verse time of day.....	130
81. (a) Temperature comparison for element 17775 (original map) verse element 4545 (map with deleted elements) for July 2 <sup>nd</sup> , 2003. (b) Difference in Temperature between the original map and the trimmed map. ....	131
82. (a) Temperature comparison for element 19009 (original map) verse element 4964 (map with deleted elements) for July 2 <sup>nd</sup> , 2003. (b) Difference in Temperature between the original map and the trimmed map. ....	132
83. (a) Temperature comparison for element 14329 (original map) verse element 3310 (map with deleted elements) for July 2 <sup>nd</sup> , 2003. (b) Difference in Temperature between the original map and the trimmed map. ....	133
84. (a) Temperature comparison for element 10832 (original map) verse element 1903 (map with deleted elements) for July 2 <sup>nd</sup> , 2003. (b) Difference in Temperature between the original map and the trimmed map. ....	134
85. (a) Temperature comparison for element 10494 (original map) verse element 1813 (map with deleted elements) for July 2 <sup>nd</sup> , 2003. (b) Difference in Temperature between the original map and the trimmed map. ....	134

## LIST OF FIGURES - CONTINUED

Figure	Page
86. (a) Temperature comparison for element 7388 (original map) verse element 810 (map with deleted elements) for July 2 <sup>nd</sup> , 2003. (b) Difference in Temperature between the original map and the trimmed map. ....	135
87. (a) Temperature comparison for element 5470 (original map) verse element 379 (map with deleted elements) for July 2 <sup>nd</sup> , 2003. (b) Difference in Temperature between the original map and the trimmed map. ....	136
88. Meteorological Plots from 12:00 am on February 2 <sup>nd</sup> , 2003 for (a) air temperature vs. time (b) solar radiation vs. time (c) cloud cover verse time of day .....	138
89. (a) Temperature comparison for element 5470 (original map) verse element 379 (map with deleted elements) for February 2 <sup>nd</sup> , 2003. (b) Difference in Temperature between the original map and the trimmed map. ....	139
90. (a) Temperature comparison between element 19009 (original map) verse element 4964 (map with deleted element) for February 2 <sup>nd</sup> , 2003. (b) Difference in Temperature between the original map and the trimmed map.....	139
91. (a) Temperature comparison between element 14329 (original map) verse element 3310 (map with deleted element) for February 2 <sup>nd</sup> , 2003. (b) Difference in Temperature between the original map and the trimmed map.....	140
92. (a) Temperature comparison between element 10832 (original map) verse element 1903 (map with deleted element) for February 2 <sup>nd</sup> , 2003. (b) Difference in Temperature between the original map and the trimmed map.....	141
93. (a) Temperature comparison between element 10494 (original map) verse element 1813 (map with deleted element) for February 2 <sup>nd</sup> , 2003. (b) Difference in Temperature between the original map and the trimmed map.....	141

## LIST OF FIGURES - CONTINUED

Figure	Page
94. (a) Temperature comparison between element 7388 (original map) verse element 810 (map with deleted element) for February 2 <sup>nd</sup> , 2003. (b) Difference in Temperature between the original map and the trimmed map.....	142
95. (a) Temperature comparison between element 5470 (original map) verse element 379 (map with deleted element) for February 2 <sup>nd</sup> , 2003. (b) Difference in Temperature between the original map and the trimmed map.....	143

## NOMENCLATURE

$A$	Area ( $m^2$ )
$C_{ak}$	Air to ground convection conductor
$C_{Ho}$	Bare soil heat transfer coefficient
$C_{kk}$	Ground layer conduction
$C_p$	Specific heat at constant pressure (J/kg-K)
$C_{Rain}$	Rain convection conductor
$CAP_{k_i}$	Heat capacitance (J/ $m^2$ -K)
$d_i$	Thickness of ground layers (m)
$E$	Emissive Power ( $W/m^2$ )
$E_b$	Emissive Power of Blackbody ( $W/m^2$ )
$F_{i-j}$	View Factor
$G$	Irradiation ( $W/m^2$ )
$h_{fg}$	Latent Heat of vaporization (J/kg)
$I_{\lambda,e}$	Emitted spectral intensity ( $W/m^2$ -K)
$I_i$	Intensity of radiation leaving surface i ( $W/m^2$ -K)
$J_i$	Radiosity ( $W/m^2$ )
$k$	Von Karmon constant
$k$	Thermal conductivity (W/m-K)
$m$	Mass (kg)

## NOMENCLATURE - CONTINUED

$n_i$	Surface normal
$n_j$	Surface normal
$N$	Number of surfaces (or elements) in an enclosure
$q$	Heat transfer rate (W)
$Q$	Heat flux (W/m <sup>2</sup> )
$r$	Distance between centers of differential areas (m).
$t$	Time (s)
$T_a$	Air temperature (K)
$T_k$	Temperature at the surface (K)
$T_R$	Rain temperature (K)
$T_s$	Absolute Temperature (K)
$u$	Specific internal energy (kJ/kg)
$U$	Total internal energy (kJ)
$v$	Average rain velocity (mm/hr)
$v_a$	Average Wind Velocity (m/s)
$w$	Soil moisture
$W$	rate at which work is performed (W)
$\omega_g$	Volume fraction of surface soil moisture
$w_k$	Volume fraction of surface soil moisture
$\alpha$	Absorptivity

## NOMENCLATURE – CONTINUED

$\varepsilon$	Emissivity
$\lambda$	Wavelength (m)
$\phi$	Azimuth angle (rad)
$\rho$	Reflectivity (Albedo)
$\rho_a$	Density of air (kg/m <sup>3</sup> )
$\tau$	Transmissivity
$\theta$	Zenith angle (rad)
$\sigma$	Stefan-Boltzmann Constant
$\omega$	Solid angle (sr)

## CHAPTER 1

## INTRODUCTION

The Western Transportation Institute (WTI) is collaborating with the Montana Department of Transportation (MDT), Meridian Environmental Technology Incorporated, The Montana Department of Federal Highways Administration, Montana State University Civil Engineering, and ThermoAnalytics Incorporated (TAI) on a project known as the Greater Yellowstone Regional Traveler and Weather Information System (GYRTWIS). Part of this project is to develop and integrate a pavement temperature thermal model to provide a more detailed temperature forecast for two mountain passes: Lookout Pass on the Montana-Idaho border and Bozeman Pass [Ballard, 2001]. The goal is to accurately provide current and forecast weather and road condition information to highway operators and users. The prediction of pavement temperatures is currently being provided to help decision makers improve winter road maintenance operations. It could also be used in the future to provide forecasts of icy conditions for travelers.

The idea for modeling sections of highway is based on the adaptation of computational models used by the U.S military for the prediction of vehicle infrared images. Two programs were developed as tools to model the surface temperatures of vehicles for use in infrared imagery. The origin of the one dimensional, first principles heat transfer software for which the pavement model is derived is the Thermal Contrast Model (TCM), initially developed for the U.S. Air Force and PRISM (Physically Reasonable Infrared Signature Mode), which was produced at Michigan Technological

University's Keweenaw Research Center in conjunction with the U.S. Army Tank-Automotive Command (TACOM) [Adams, 1999]. Basically, the infrared signature of a vehicle exposed to a set of meteorological conditions indicates the surface temperature of the vehicle. The three-dimensional modeled vehicles were composed of a collection of flat plates termed "facets". The terrain in the model was considered as background and originally represented as an isothermal, flat plate. The facet concept used for vehicles was extended and used to represent the terrain presently used in the thermal modeling software [Adams and McDowell, 1991].

The current modeling tool used to predict these surface temperatures is a Radiation based Thermal Model for Road Temperature (RadTherm/RT). RadTherm/RT is a thermal modeling tool intended for comprehensive heat management design and analysis. ThermoAnalytics developed the software in conjunction with Montana State University to predict and graphically display road and surrounding terrain temperatures. The software provides a tool to analyze and model terrain temperature utilizing 3-D radiation, convection, and 1-D conduction. The input into the software includes a digital 3D-faceted terrain representation, meteorological data, and time/location information.

Developments in Geographic Information Systems (GIS), and the availability of Digital Elevation Maps (DEM) make it possible to produce files for elevation, road, and vegetation maps. The vegetation in this context includes grass, forests, water, rock, soil, etc. The elevation data was compiled from a United States Geological Survey (USGS) DEM's at a 30-meter resolution. The weather file includes standard meteorological parameters such as air temperature, wind velocity, precipitation, relative humidity, and

radiation data. From USGS DEM's, the mesh of the model was created in 30-meter square sections. Once the files were loaded into RadTherm/RT the sections were further divided into triangular elements. The output from RadTherm/RT is the temperature map for each node in the system.

The first step in constructing the thermal model is to fabricate maps for the region of interest [Adams, 1999]. Interstate 90 through Bozeman Pass will be the area of focus for this thesis. Geographic Information Systems (GIS) experts from Montana State University's Geographic Information and Analysis Center (GIAC) produced the ASCII files for the elevation, road and vegetation maps using ARC/INFO GIS software. The U.S. Geologic Survey provides the digital elevation maps as the source for the elevation file. The terrain file is simply the GIS vegetation ID's from the land cover class and is converted to RadTherm/RT part numbers used to group land covers with similar engineering properties, including emissivity, absorptivity, thermal conductivity, etc.

The elevation and terrain files are loaded into RadTherm/RT to create a new project. However, there is a limitation on the size of a thermal map that can be processed. As the boundaries of the thermal map increase, the number of elements also increases. At a certain point, the calculations for the thermal solution become too complex for computers to solve. Therefore, to optimize the models, a methodology to optimize the number of elements without changing the dimensions of the thermal map was considered beneficial.

One attempt to reduce the size of the thermal map was with the use of a topographic map. The goal was to eliminate the maximum number of elements while keeping all important terrain features that could cause temperature changes on the highway by shade,

radiation exchange, etc. The major concern for this approach is the lack of standards for reducing the boundaries of the map. For example, if a pertinent terrain attribute, such as a mountain peak, is deleted it could greatly influence the temperature output of the terrain or road.

Another method to increase the efficiency of the thermal maps combine the efforts of Montana State University and ThermoAnalytics, Inc. The DEM and vegetation file produced by GIAC for Bozeman Pass is sent to ThermoAnalytics, Inc. to be remeshed. This process includes combining terrain elements to reduce the number of nodes in the map. For instance, four 30-meter square elements are combined to create a single 60x60-meter square element. There are two disadvantages of this process. First, by combining elements, different thermal properties are lost and inaccuracies may be introduced. Second, coarsening the map can be a time-consuming task.

For this project, an analytical approach to optimize the elements used for thermal maps in RadTherm/RT was developed. Chapter 2 gives an overview of heat transfer principles and develops the equations used in the software. View factors are introduced and explained as the basis for eliminating elements for this methodology. A view factor is the fraction of energy that leaves one surface and is absorbed at a second surface. ThermoAnalytics' software determines the radiation relationships between elements that are visible to one another in the model and to the environment [[www.thermoanalytics.com](http://www.thermoanalytics.com)]. This algorithm is explored in detail in Chapter 3.

A simple model is introduced in Chapter 3 to describe the energy exchange between elements in different scenarios. The view factors are shown for different orientations and

resulting temperatures are compared. Conclusions from the example demonstrate that energy exchange is highly dependent on angle of slope, distance, and the material surface.

The next section of Chapter 3 describes a detailed methodology used to reduce the number of elements from a thermal map. A four-part C/C++ code was implemented to complete this task. This process is designed to be universal for any region of interest. The goal of this thesis is to significantly reduce the number of elements to improve the efficiency of the map without sacrificing accuracy. This would allow longer stretches of highway to be run with minimal computation time.

## CHAPTER 2

### BACKGROUND

#### Heat Transfer

Thermal energy is related to the temperature of matter. The higher the temperature of a material of given mass, the greater its thermal energy. Heat transfer is the exchange of thermal energy through a body or between bodies and occurs when there is a temperature difference. When a temperature gradient exists between two bodies, thermal energy transfers from the one with a higher temperature to the one with a lower temperature.

There are three modes of heat transfer: conduction, convection, and radiation. Any energy exchange between bodies occurs through one of these modes or a combination of them [Incropera and DeWitt, 1996]. The following section gives a brief introduction to each mode.

#### Conduction

The definition of conduction is the transfer of energy from the more energetic to the less energetic particles of a substance due to interactions between the particles. When there exists a temperature gradient, energy transfer by conduction will occur in the direction of decreasing temperature [Incropera and DeWitt, 1996]. The rate of heat flow due to conduction increases with the thermal conductivity of the material, the cross-sectional area available for it to pass through, and the temperature difference from one

side to the other. As material thickness increases, due to the increased path length, the longer it takes the heat to “flow” from one side to another.

### Convection

Convection is heat transfer by mass motion of a fluid such as air or water when the heated fluid is caused to move away from the source of heat, carrying energy with it. Natural convection above a hot surface occurs when hot air expands it becomes less dense, and rises. On the other hand, forced convection is caused by something external such as atmospheric winds or a fan. RadTherm/RT uses the flat plate assumption to calculate the forced convective heat transfer. This is highly dependent on wind speed and temperature difference between the air and surface.

### Radiation: Processes and Properties

Radiation is the transfer of energy in the form of electromagnetic waves. This radiation is emitted by objects in all directions without the need of a solid or fluid to transfer the heat [Incropera and DeWitt, 1996]. It uses electromagnetic radiation (photons), which travels at the speed of light and is emitted by any matter with temperature above zero degrees Kelvin (-273 °C). The main types of radiation (from short to long wavelengths) are; gamma rays, X-rays, ultraviolet (UV), visible light, infrared (IR), microwaves, and radio waves. The electromagnetic spectrum classifies radiation according to wavelengths. High-energy physicists and nuclear engineers are primarily concerned with the short wavelength gamma rays, X rays, and UV radiation, while electrical engineers focus on the longer wavelength microwaves and radio waves

[Incropera and DeWitt, 1996]. Thermal radiation is given off by all surfaces that surround us and is in band wavelengths from 0.1 to 100  $\mu\text{m}$  in the electromagnetic spectrum [Sparrow, 1970]. The complete electromagnetic spectrum is illustrated in Figure 1.

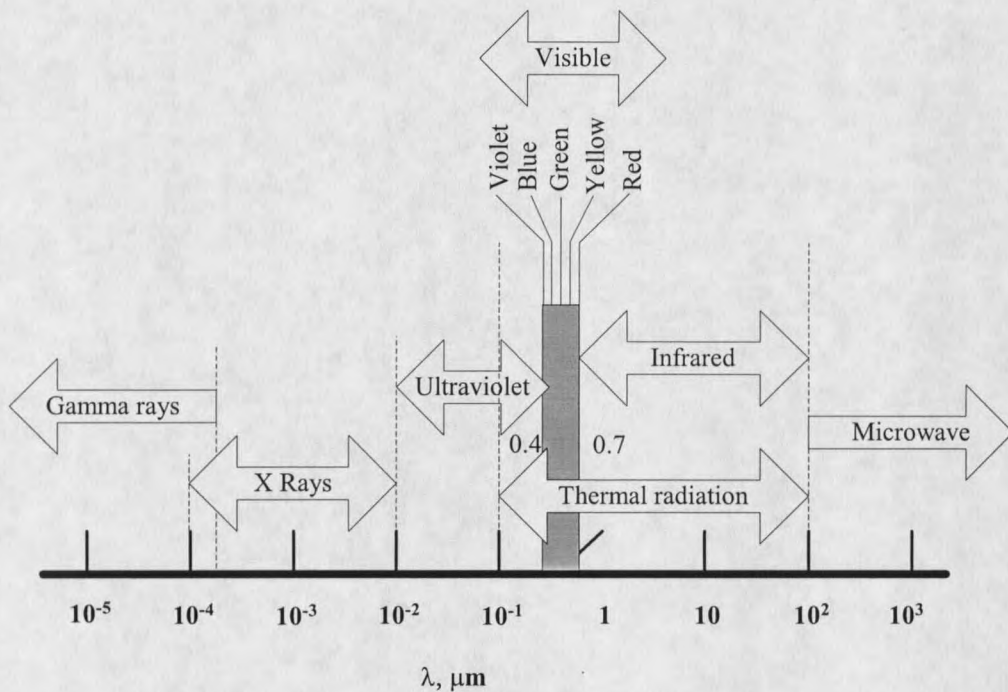


Figure 1. Electromagnetic Spectrum (After Incropera and DeWitt, 1996, Figure 12.3)

Radiation with shorter wavelengths is more energetic. The temperature of the body largely determines the type of radiation emitted. Very hot objects, such as the sun at  $\sim 5800$  K, emit more energetic radiation including visible and UV. For engineering applications, radiated power is usually in infrared, and sometimes visible or UV. Radiation can be emitted, absorbed, transmitted and reflected by matter (solid, liquid and gas) and can be broken into two parts, shortwave and longwave [Sparrow, 1970].

Shortwave Radiation. The primary source of energy forcing atmospheric motion and many different processes in the atmosphere, at the Earth's surface and in the oceans, is the radiant energy from the sun [Pluss, 1997]. The radiation emitted by the sun is approximately equal to the emission of a blackbody at 5750 K. More than 99% of the energy received from the sun at the top of the earth's atmosphere is in the wavelength range 0.2 to 4.0  $\mu\text{m}$  and known as shortwave radiation [Pluss, 1997]. Shortwave (or Solar) radiation reaches the earth's surface either by being transmitted directly through the atmosphere, direct solar radiation, or by being scattered or reflected to the surface, known as diffuse solar radiation. Diffuse solar radiation is scattered by air molecules, aerosol particles, cloud particles, or other particles.

About 50 percent of shortwave radiation is reflected back into space, while the remaining shortwave radiation at the top of the atmosphere is absorbed by the earth's surface and re-radiated as thermal infrared, or longwave radiation [Pluss, 1997].

Longwave Radiation. Hot objects like the sun emit radiation in shorter wavelengths, while colder bodies, such as the Earth or Earth's atmosphere, emit radiation in longer wavelengths ranging from 4.0 to 100.0  $\mu\text{m}$ . Most longwave radiation reaching the earth surface is emitted from the lowest layers of the atmosphere. The main emitter of incoming longwave radiation is the greenhouse of the earth (e.g. water vapor, carbon dioxide, and ozone) [Pluss, 1997]. Longwave radiation is created from the temperature difference between the atmosphere and the earth's surface. On a clear day the atmosphere is much cooler than the earth's surface and energy is emitted from the surface to the sky.

### Radiation Exchange Between Surfaces

All bodies above absolute zero Kelvin temperature radiate energy. Substances emit and absorb radiant energy at a rate depending on the absolute temperature and physical properties of the substance. Not only do they radiate or emit energy, but they also receive and absorb it from other sources [Beckwith, et al, 1993]. Two sets of criteria govern radiative heat transfer between surfaces. The first depends on the material properties, including emissivity, absorptivity, and reflectivity with each depending on temperature.

The second consists of the geometry and the transmission of radiation as a function of direction from the surface and the wavelength of the emitted radiation. This is calculated by the use of view factors. The study of radiation heat transfer in engineering is concerned with the heat loss by emission and heat gain by absorption.

Surface Absorption, Reflection, and Transmission. Incoming shortwave (or solar) radiation that strikes the earth's surface is partially reflected and partially absorbed, in proportion to the surface reflectivity. Figure 2 describes the absorbed, reflected, and transmitted radiation with a semitransparent medium. These incoming portions are divided into fractions of absorptivity ( $\alpha$ ), reflectivity ( $\rho$ ), and transmissivity ( $\tau$ ), where

$$\alpha + \rho + \tau = 1. \quad (1)$$

Absorptivity is defined as the fraction of incident radiation (or irradiation) absorbed by an object in relation to a blackbody (range 0-1). Irradiance is the amount of electromagnetic energy incident on a surface per unit time per unit area. This quantity is often referred to as "flux" [Ozisik, 1977].

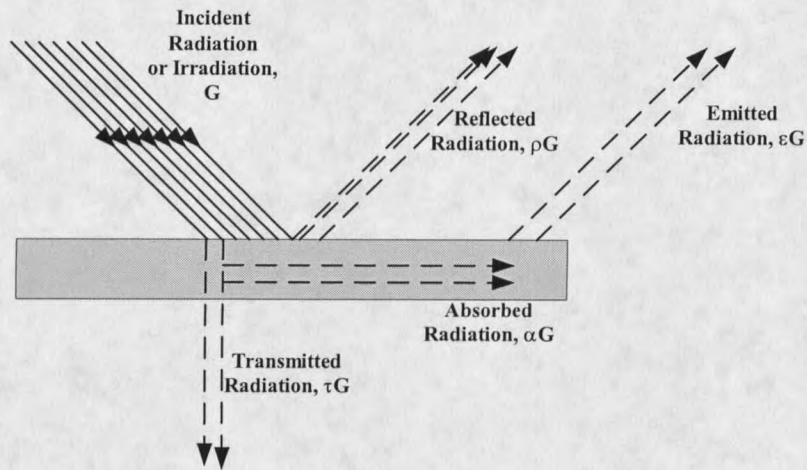


Figure 2. Absorbed, reflected, and transmitted shortwave radiation with a semitransparent medium.

A blackbody is any object that completely absorbs any heat or light radiation falling upon it. Reflectivity (or albedo) is the ratio of the reflected solar radiation divided by incoming solar radiation, incident upon a surface. Transmissivity is a property that is dependent on the temperature of the body and the wavelength of the incident radiation. It is a dimensionless value and measured as the fraction of incident radiation that is transmitted through the body [Ozisik, 1977].

A highly polished surface is referred to as an ideal reflector, where reflectivity ( $\rho$ ) approaches 1 ( $\rho \rightarrow 1$ ). Many gases represent substances of high transmissivity, for which  $\tau \rightarrow 1$ . An example of an ideal absorber, or blackbody, is a small opening into a large cavity, for which  $\alpha \rightarrow 1$  [Beckwith, et al, 1993]. For opaque solid bodies, such as soil, rock, or highway the transmissivity component can be ignored and Equation (1) is

written as,

$$\alpha + \rho = 1. \quad (2)$$

Surface Emission. The rate at which energy is released per unit area by a surface is known as the emissive power  $E$  [Incropera and DeWitt, 1996]. At a prescribed temperature and wavelength, no surface emits more than a blackbody. The total emissive power of a blackbody and the upper limit of emissive power is specified by the Stefan-Boltzmann law,

$$E_b = \sigma T_s^4, \quad (3)$$

where  $\sigma$  is the Stefan-Boltzmann constant ( $\sigma = 5.67 \times 10^{-8} \text{ W / (m}^2 \text{K}^4)$ ) and  $T_s$  is the absolute temperature (K) of the surface. The heat flux emitted by a real surface is less than that of a blackbody and dependent on the surfaces' emissivity value,

$$E = \varepsilon \sigma T_s^4. \quad (4)$$

Emissivity is a characteristic of a surface that determines its ability to emit heat by radiation [Ozisik, 1977]. It is a ratio of the amount of energy an object absorbs and reradiates versus amount of energy a perfect emitter or black body would radiate under the same conditions (range 0-1).

View Factor. The Stefan-Boltzman Equation (3) provides a method of determining the total energy leaving a surface, but gives no indication of the direction in which it travels. Since the goal is to calculate how heat is distributed among various objects, a second phenomenon is introduced that governs radiative heat transfer between surfaces. The geometric effects are introduced and these are described by the view factor (also

called a configuration or shape factor),  $F_{ij}$ , and are therefore important in computing the radiation exchange between any two surfaces. By definition, the view factor  $F_{ij}$  is the fraction of the radiation leaving surface  $i$  that is intercepted by surface  $j$ .

To develop a general expression for  $F_{ij}$ , consider three fluxes of thermal radiation, called emissive power, irradiation, and radiosity. First consider radiative emission from a surface (emissivity), which has both directional and spectral wavelength dependencies, is schematically shown in Figure 3.

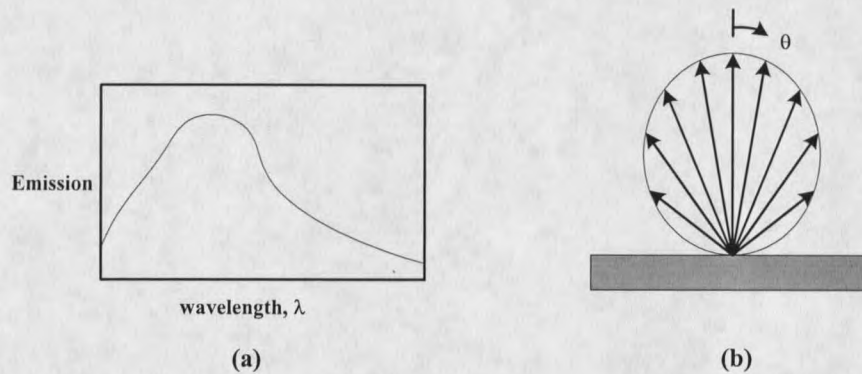


Figure 3. Radiation emitted by a surface. (a) Spectral distribution. (b) Directional distribution. (After Incropera and DeWitt, 1996, Figure 12.4)

Since radiation can potentially emit in all directions, it is most convenient to develop the mathematics in a spherical coordinate system, as illustrated in Figure 4. The differential element  $dA_1$  on the surface of a material emits thermal radiation. The surface-normal direction is indicated by the unit vector  $n$ , and  $\theta$  is the zenith angle from the surface normal.

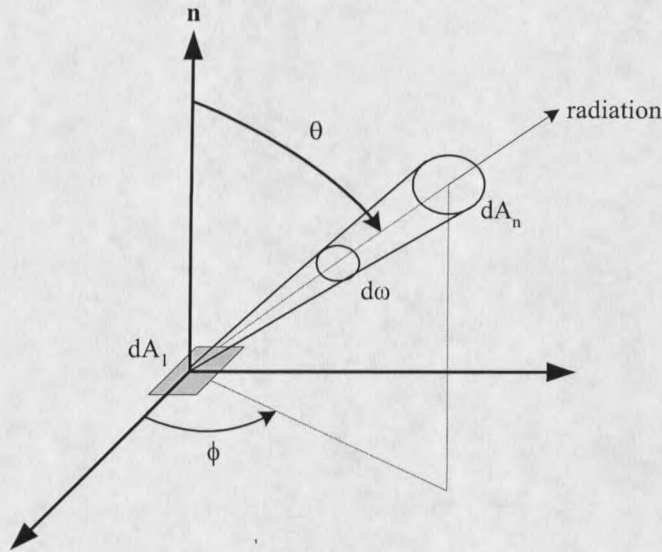


Figure 4. Radiation emitted from a point in differential area  $dA_1$  into a solid angle  $d\omega$  subtended by differential area  $dA_n$ . (After Incropera and DeWitt, 1996, Figure 12.5)

The radiation passes through a differential area  $dA_n$  that is normal to a ray emanating from the surface element  $dA_1$  at angles  $\theta$  and  $\phi$  of the spherical coordinate system. The differential solid angle  $d\omega$  is formed from a ray  $r$  connecting the center of  $dA_n$  to the center of  $dA_1$ . The differential solid angle subtended by  $dA_n$  from a point on the surface  $dA_1$  depends on two things. First, the distance  $r$  between centers of the differential areas and second, the area segment of a spherical surface  $dA_n$  that projects normal to the connecting ray between  $dA_1$  and  $dA_n$ . As seen in Figure 5a, the differential plane angle  $d\alpha$  is defined by a section between the rays of a circle and is measured in terms of arc length  $dl$  on the circle to the radius  $r$  of the circle [Incropera and DeWitt, 1996],

$$d\alpha = \frac{dl}{r}. \quad (5)$$

This is often used to find an arc length ( $dl$ ), where

$$dl = r \cdot d\alpha. \quad (6)$$

The idea of an angle and arc length is taken to three dimensions to define a differential solid angle,  $d\omega$ . When the solid angle is multiplied by the radius squared, it has dimensions of length squared, or area, and will have the magnitude of the differential area ( $dA_n$ ), where

$$dA_n = r^2 \cdot d\omega. \quad (7)$$

Solving Equation (7) for  $d\omega$  yields

$$d\omega = \frac{dA_n}{r^2}. \quad (8)$$

A solid angle is shown in Figure 5b.

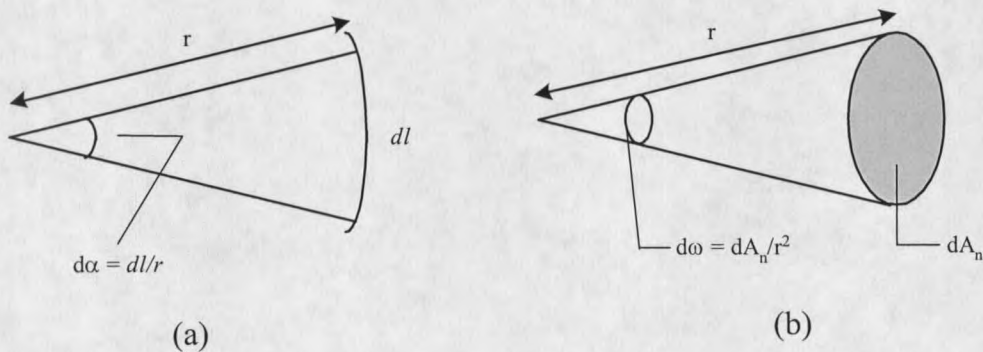


Figure 5. (a) Definition of a plane angle. (b) Definition of a solid angle. (After Incropera and DeWitt, 1996, Figure 12.6)

Since  $dA_n$  is a segment of a spherical surface, normal to the  $(\theta, \phi)$  direction, as shown in Figure 6,  $dA_n$  may be represented as the following

$$dA_n = r^2 \sin \theta \, d\theta \, d\phi. \quad (9)$$

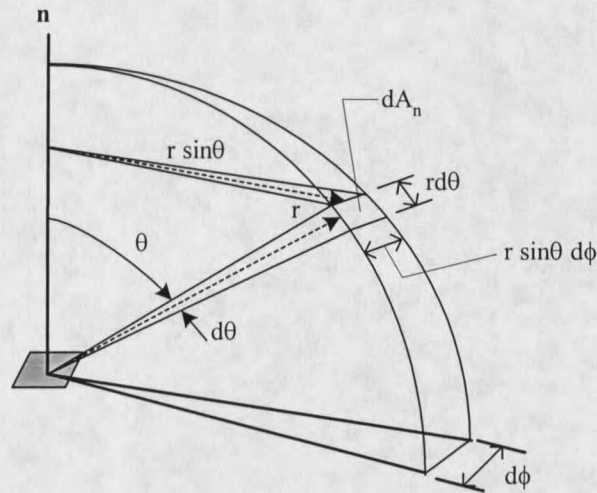


Figure 6. In the spherical coordinate system, a solid angle subtended by  $dA_n$  from a point on  $dA_1$ . (After Incropera and DeWitt, 1996, Figure 12.7)

Then, from the definition of  $d\omega$ , it is clear that

$$d\omega = \sin \theta \cdot d\theta \cdot d\phi \quad (10)$$

The above definitions are important when considering how energy radiates from a point source. Next, consider the rate at which emission from  $dA_1$  passes through  $dA_n$  as seen in Figure 4. Consider two infinitesimal elements of two surfaces  $dA_i$  and  $dA_j$  as seen in Figure 7. Each surface has a normal vector  $n_i$  and  $n_j$ , and the normals make angles  $\theta_i$  and  $\theta_j$  with the line connecting the two elements (Figure 7).

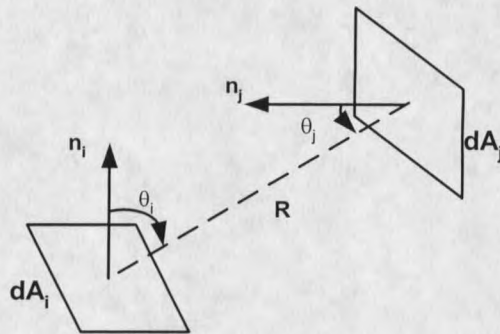


Figure 7. Two surface normals of the differential areas  $dA_i$  and  $dA_j$ .  $\theta_i$  and  $\theta_j$  are the angles to the line connecting the two bodies.

A variable called emitted spectral intensity,  $I_{\lambda,e}(\lambda, \theta, \phi)$ , is defined as the “rate at which radiant energy is emitted at the wavelength  $\lambda$  in the  $(\theta, \phi)$  direction, per unit area of the emitting surface normal to this direction, per unit solid angle around this direction, and per unit wavelength interval  $d\lambda$  about  $\lambda$  [Incropera and DeWitt, 1996]. To illustrate “per unit area of emitting surface normal to this direction” refer to Figure 8.

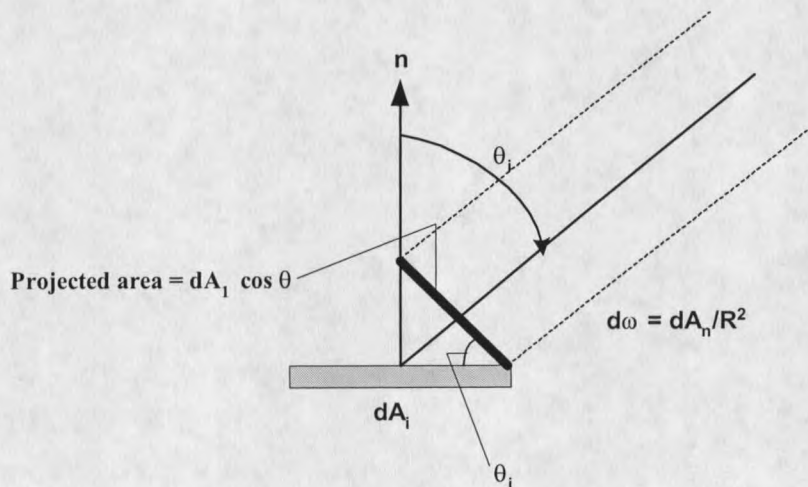


Figure 8. The projection of  $dA_i$  and  $dA_j$  normal to the direction of radiation.

The emitted spectral intensity is defined to account for the way in which an observer situated along an emitted ray would see  $dA_i$ . The differential area  $dA_n$  is normal to a ray emitting at an angle  $\theta_i$ . The projected view of  $dA_i$  is  $dA_i \cos \theta_i$ . As  $\theta_i$  approaches  $\pi/2$ , the view of  $dA_i$  is reduced until  $\theta = \pi/2$  and at this point the projected view ( $dA_n$ ) is zero. This is an important point because even if a surface is very hot, i.e., has a high emitted intensity, an observer viewing at a very low, shallow angle will receive very little energy from the surface. This reduced transfer is due to the small area through which the energy may be projected to the observer.

Figure 9 demonstrates the next part of the spectral intensity definition “per unit solid angle around this direction”.

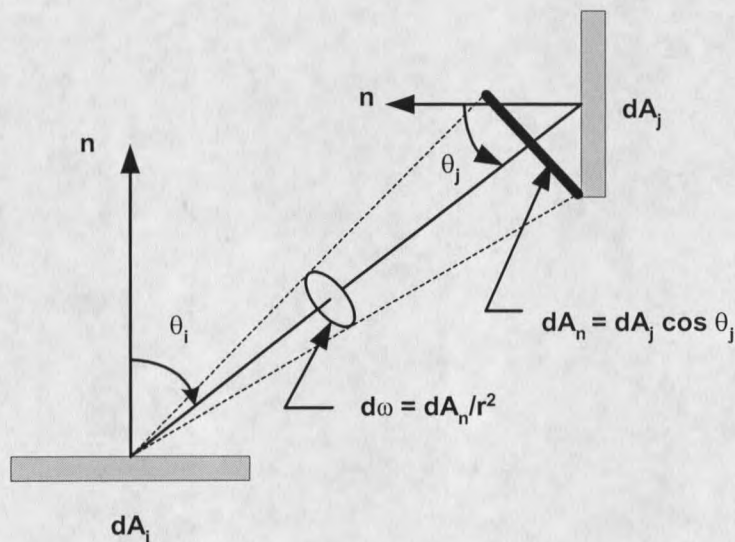


Figure 9. The differential solid angle subtended by  $dA_j$  from a point on  $dA_i$ .

The differential solid angle  $d\omega_{j-i}$  subtended by  $dA_j$  relative to a point on  $dA_i$  depends on the distance between the centers of the differential areas  $r$  and the area  $dA_n$  that  $dA_j$  projects normal to the connecting ray between  $dA_i$  and  $dA_j$ .

$$d\omega_{j-i} = \frac{dA_n}{r^2} = \frac{dA_j \cos \theta_j}{r^2} \quad (11)$$

The emitted spectral intensity is defined as

$$I_\lambda(\lambda, \theta, \phi) = \frac{dq}{dA_i \cos \theta d\omega d\lambda}, \quad (12)$$

and

$$dq_\lambda = \frac{dq}{d\lambda}, \quad (13)$$

where  $dq$  is the rate at which radiation is emitted. Using the definition in Equation (13), Equation (12) is solved for  $dq_\lambda$ , which is the rate at which radiation of wavelength  $\lambda$  leaves  $dA_i$  and passes through  $dA_n$ ,

$$dq_\lambda = I_\lambda(\lambda, \theta, \phi) dA_i \cos \theta d\omega \quad (14)$$

This equation can be simplified if the emitting surface is a gray surface. A surface is gray if its emissivity and absorptivity are independent of wavelength, for the wavelengths at which irradiation and emission take place. Applying the assumption of a gray surface, Equation (14) can be written as the radiation from surface  $i$  and intercepted by  $j$ :

$$dq_{i-j} = I_i(\theta_i, \phi_i) (dA_i \cos \theta_i) d\omega_{j-i}, \quad (15)$$

where  $I_i$  is the intensity of radiation leaving surface  $i$ . Applying Equation (11), Equation (15) becomes

$$dq_{i-j} = I_i(\theta_i, \phi_i)(dA_i \cos \theta_i) \left( \frac{dA_j \cos \theta_j}{r^2} \right). \quad (16)$$

This shows that as an observer moves farther and farther from a given heat surface (i.e., increasingly large  $r$ ), the amount of energy or heat received will be reduced because of the  $r^2$  term in the denominator. Equation (16) can be reduced further if all visible light sources are diffuse emitters and all surfaces are diffuse reflectors. For a diffuse reflector an incoming ray of light is equally likely to be reflected in any direction over the hemisphere as in Figure 10.

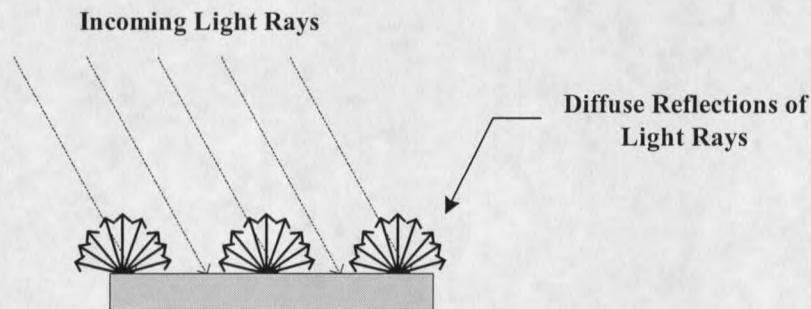


Figure 10. A diffuse reflector.

A diffuse emitter is a surface that emits radiation equally in all directions, analogous to reflections shown in Figure 10.

Therefore, the radiation for a diffuse surface,  $I_i(\theta_i, \phi_i)$ , is not dependent on direction  $(\theta_i, \phi_i)$  and gives a relationship between the radiation intensity,  $I_i$ , and the radiosity  $J_i$ ,

$$I_i = \frac{J_i}{\pi}. \quad (17)$$

Note that the radiation flux, in this case the radiosity, is based on the actual surface area, while the intensity is based on the projected area. The radiosity,  $J_i$ , from a surface ( $i$ ) is the sum of the emissive power and the reflected part of the irradiation as shown in Figure 11.

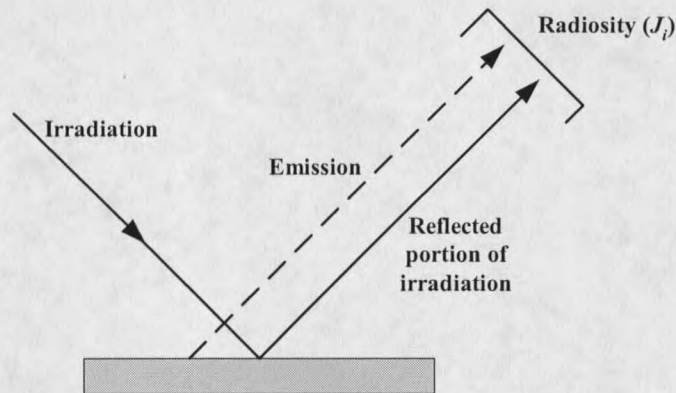


Figure 11. Surface radiosity.

Any body that has a temperature above absolute zero emits energy in the form of thermal radiation flux, which is called the Emissive Power,  $E$ . The irradiation  $G$  is defined as the flux incident on a surface, usually as the result of emissive power or radiosity from another surface.

Substituting Equation (17) into Equation (16) yields

$$dq_{i-j} = J_i \frac{\cos \theta_i \cos \theta_j}{\pi r^2} dA_i dA_j. \quad (18)$$

The total rate at which radiation leaves surface  $i$  and is intercepted by  $j$  is obtained by integrating over the two surfaces. Note that the radiosity  $J_i$  is uniform over the surface  $A_i$ ,

$$q_{i \rightarrow j} = J_i \int_{A_i} \int_{A_j} \frac{\cos \theta_i \cos \theta_j}{\pi r^2} dA_i dA_j. \quad (19)$$

Using the definition of a view factor as the fraction of the radiation that leaves  $A_i$  and is intercepted by  $A_j$ ,

$$F_{i \rightarrow j} = \frac{q_{i \rightarrow j}}{A_i J_i}. \quad (20)$$

Substituting Equation (19) into Equation (20) gives us the view factor equation,

$$F_{i \rightarrow j} = \frac{1}{A_i} \int_{A_i} \int_{A_j} \frac{\cos \theta_i \cos \theta_j}{\pi r^2} dA_i dA_j. \quad (21)$$

In a similar manner the view factor from  $A_j$  to  $A_i$  is found to be

$$F_{j \rightarrow i} = \frac{1}{A_j} \int_{A_j} \int_{A_i} \frac{\cos \theta_i \cos \theta_j}{\pi r^2} dA_i dA_j. \quad (22)$$

An important relation is the reciprocity for view factors between finite areas. The double integrals in Equation (21) and Equation (22) are identical and therefore gives us the reciprocity relation

$$A_i F_{ij} = A_j F_{ji}. \quad (23)$$

A second important relation relates to surfaces in an enclosure. From conservation of energy requirements, all radiation leaving any surface in the enclosure must be intercepted by a surface making up the enclosure. When this is applied to  $N$  surfaces in

an enclosure, the fraction of energy leaving one surface and reaching surfaces of the enclosure must total to unity [Incropera and DeWitt, 1996],

$$F_{i-1} + F_{i-2} + F_{i-3} + \cdots + F_{i-i} + \cdots + F_{i-N} = \sum_{j=1}^N F_{i-j} = 1. \quad (24)$$

The term  $F_{i-i}$  is included in the summation because when a surface is concave, it will intercept a part of its own emitted energy. On the other hand, for a plane or convex surface,  $F_{i-i}$  is zero.

#### RadTherm/RT Heat Transfer

RadTherm/RT is a thermal modeling program developed to predict surface terrain and road temperatures. Inputs into the software include a digital elevation map, a vegetation map, meteorological data, and time/location information [ThermoAnalytics, 1999]. The vegetation map includes different types of vegetation, rock, soil, and road information. A RadTherm/RT project includes a region of interest that is composed of a number of parts. Every part will have one or more elements associated with it and a thermal node is assigned to each element. Parts are collections of elements that have the same material properties. For example, short grass is considered a separate part from the interstate. The thermal results are solved for the individual elements, but all properties including part type, materials, thickness, convection coefficient, etc., are assigned at the part level. The properties applied to a part, are applied to all of the elements assigned to the part [ThermoAnalytics, 2000].

Every element has one or more thermal nodes, depending on the part type that has been chosen for the particular element. For this project, only terrain elements were considered. Therefore, each element in the mesh is modeled as having one surface (front) and a single thermal node is associated with the surface of each element. The thermal results are calculated for each of these nodes [ThermoAnalytics, 2000].

The geometry of a map is divided into a two-dimensional grid, where each rectangular element of the grid is divided into two triangular terrain elements. The following example uses a quadrilateral element for simplicity of discussion. Figure 12 shows a map of Bozeman Pass and a section of the map broken into quadrilateral elements, each with a thermal node and an assigned part ID.

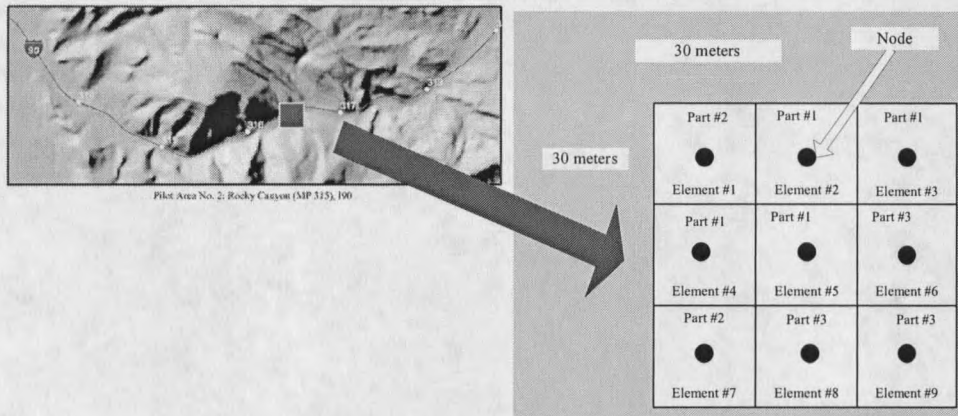


Figure 12. A mesh created for RadTherm/RT for a region of interest.

Terrain elements can be used to model several types of surfaces in RadTherm/RT including asphalt, concrete, foliage, soil, water, swamp, or snow. Each surface type is

divided into a more detailed part types, which include an interstate road, deciduous trees, short grass, rocky field, or fresh snow. These detailed part types are used to assign material properties for emissivity, absorptivity, conductivity, etc.

To develop the energy balance for a particular node, consider a single soil-type terrain element as in Figure 13.

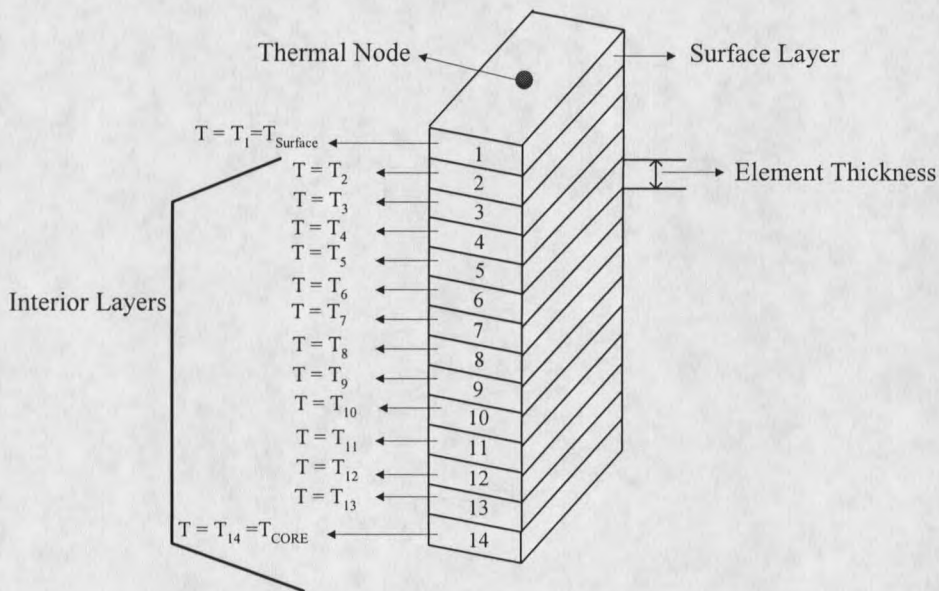


Figure 13. A single soil element and the associated layers.

The soil model is an energy balance solution for solving the surface temperature, as well as the interior layers, for seven different varieties of soil type under moisture conditions ranging from completely dry to saturated. The model consists of thirteen layers with varying properties dependent on soil type and water content [ThermoAnalytics, 1999]. The fourteenth soil layer has a known temperature called the core temperature and will be further described later in this section.

The governing equations are determined for each node. RadTherm/RT uses all modes of heat transfer including conduction, convection, and radiation in order to solve the temperature of a particular surface node. Figure 14 shows the modes for a particular surface element.

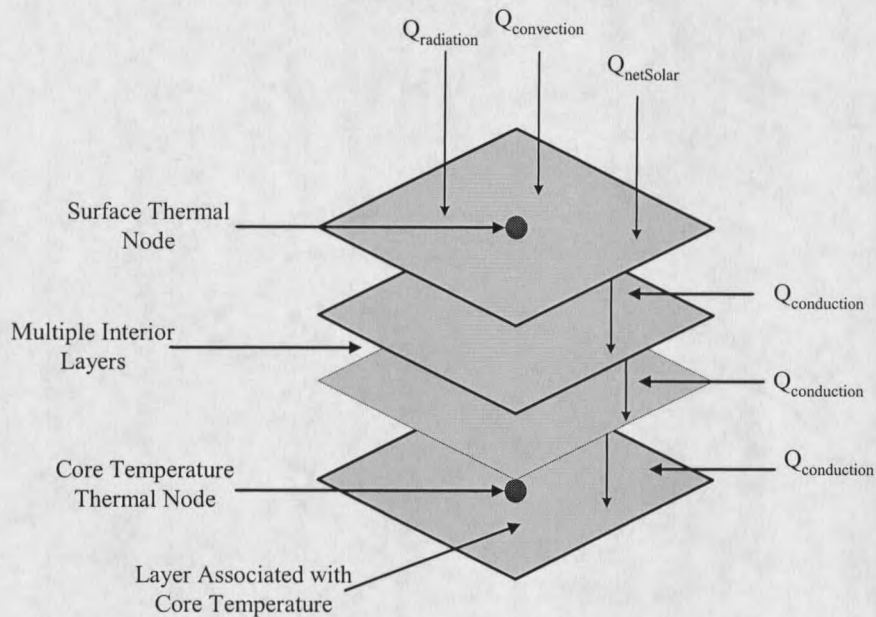


Figure 14. Heat transfer modes for each node.

The governing equations for the model are the transient energy equations and the net-radiation enclosure equation. The first law of thermodynamics is used to obtain the transient energy equation for Figure 14,

$$\frac{\partial}{\partial t} \Delta E = q - W . \quad (25)$$

The mechanical work rate (i.e. power) is denoted as  $\dot{W}$ ,  $q$  is the net heat transfer rate across the system boundary (W),  $t$  is time, and  $\Delta E$  is the change in the sum of potential, kinetic, and internal energy as

$$\frac{\partial}{\partial t} \Delta E = \frac{\partial}{\partial t} (\Delta PE + \Delta KE + \Delta U), \quad (26)$$

where  $PE$  is the potential energy,  $KE$  is the kinetic energy,  $U$  is the internal energy, and  $t$  is time. Mechanical work effects such as friction are neglected and therefore,  $\dot{W} = 0$ . Since the model forms a stationary closed system, the changes in kinetic and potential energies are negligible, so  $\Delta PE = \Delta KE = 0$  [Cengel and Boles, 1994]. Therefore, the change in stored energy,  $\Delta E$ , is only a function of total internal energy,  $U$  (kJ), and can be further simplified and expressed in terms of the specific internal energy,  $u$  (kJ/kg):

$$\frac{\partial}{\partial t} \Delta E = \frac{\partial}{\partial t} \Delta U = \frac{\partial}{\partial t} (m \Delta u) = \rho A d \frac{\partial}{\partial t} \Delta u, \quad (27)$$

where  $m$  is the mass,  $\rho$  is density,  $A$  is area, and  $d$  is the thickness of the material. Since only temperature is considered (i.e. not deformation, etc.), internal energy can be written as the specific heat,  $C_p$  (J/kg-K), times the temperature,  $T$  (K), yielding

$$\rho A d \frac{\partial}{\partial t} \Delta u = \rho A d C_p \frac{\partial T}{\partial t}. \quad (28)$$

Applying the simplifications above, the first-law in Equation (25) yields

$$\rho \cdot C_p \cdot \frac{\partial T}{\partial t} \cdot d \cdot A = q \quad (29)$$

Equation (29) will be expanded to get the energy balance equations for the interior layers as well as the surface layer. An additional development of the view factor equation will

also be discussed in the following section because it is an important concept when dealing with radiation exchange between surfaces.

### Interior Layer Energy Balance

The only heat transfer in the interior ground layers is conduction. Equation (29) becomes

$$CAP_{k_i} \cdot A_k \cdot \frac{\partial T}{\partial t} = q_{conduction} \cdot \quad (30)$$

$$CAP_{k_i} = (\rho C_p (w_i)) d_i, \quad (31)$$

for the interior layer energy balance, where  $CAP_{k_i}$  is the heat capacitance term,  $\rho$  is density ( $\text{kg/m}^3$ ), the volumetric concentration of soil moisture is defined as  $w$ ,  $A_k$  is the area of the  $k^{\text{th}}$  element ( $\text{m}^2$ ),  $d_i$  is the thickness of each interior layer (m), and  $q_{conduction}$  is the conduction heat rate (W). The notation for the subscript  $k_i$  is used to distinguish between the surface node and its associated layers. The  $k$  in subscript  $k_i$  denotes the surface element number and the subscript  $i$  in  $k_i$  indicates the interior node number in the  $k^{\text{th}}$  element. Throughout this thesis, the term  $T_k$  without the subscript  $i$  is used to represent  $T_{k_i}$ , which is the temperature of the surface node in element  $k$ . The conduction term in Equation (30) is further expanded to yield the transient energy equation for each interior thermal node of the  $k^{\text{th}}$  element. The energy balance in this case becomes

$$CAP_{k_i} \cdot A_k \cdot \frac{\partial T_{k_i}}{\partial t} = (T_{k_{i-1}} - T_{k_i}) \cdot A_k \cdot C_{kk_{i-1}} + (T_{k_{i+1}} - T_{k_i}) \cdot A_k \cdot C_{kk_i} \quad (32)$$

$$\text{for } i = N_{Layers}, T_{N_{Layers}+1} = T_{coreTemp}$$

$$C_{kk_i} = \frac{k(w_i)}{d_i} \quad (33)$$

is simple one-dimensional conduction relationship between the nodes above and below the current layer. In Equation (32),  $C_{kk_i}$  is the interior layer conduction where the thermal conductivity term  $k$  is a function of the soil moisture,  $w$ .  $N_{Layers}$  represents the number of layers for the particular terrain type. When  $i=1$  the  $T_{k_i}$  term is the surface temperature of the  $k^{\text{th}}$  element. For the case of a soil element,  $N_{Layers}$  is thirteen. The model includes an additional node,  $N_{Layers} + 1$ , as seen in Figure 13 which is used to define a known core temperature, also known as the diurnal depth temperature. This diurnal depth is the depth at which the ground does not change over a 24-hour (diurnal) period [ThermoAnalytics, 1999].

### Surface Energy Balance

The energy balance for the terrain surface layer consists of six terms: net sky radiation exchange, air convection, precipitation convection, solar load, and interior ground layer conduction. These terms are set equal to the internal energy storage term, which is the time rate of change of temperature times the heat capacitance [Terrain Manual].

Expanding the terms in Equation (29) for surface node  $k$  yields:

$$CAP_{k_1} A_k \frac{\partial T_k}{\partial t} = \left[ q_{convection_k} + q_{conduction_k} + q_{radiation} + q_{netSolar_k} + q_{Rain_k} \right] \quad (34)$$

In Equation (34),  $CAP_{k_1}$  is the surface layer capacitance,  $T_k$  is the surface node temperature,  $A_k$  is the area of element  $k$  ( $m^2$ ), and  $q$  represents the heat rate (W).

Energy Storage. The thermal capacitance is a function of the current moisture level and soil type, i.e.,

$$CAP_{k_1} = (\rho C_p (w_1)) d_1, \quad (35)$$

where  $w_1 = w_g$ . In Equation (35) the volumetric concentration of soil moisture is defined as  $w$ . The term  $w_g$  is the volume fraction of surface soil moisture,  $d_1$  is the surface layer thickness, and  $\rho$  is the density.

Air Convection. The convection between the air and ground is represented as

$$q_{convection_k} = (T_a - T_k) \cdot A_k \cdot C_{ak}, \quad (36)$$

where  $T_a$  is the air temperature,  $A_k$  is the area of element  $k$ , and  $T_k$  is the temperature of the surface. The variable  $C_{ak}$  represents the air to ground convection conductor and defined as

$$C_{ak} = \rho_a C_{p,a} C_{Ho} v_a, \quad (37)$$

where  $\rho_a$  is the density of the air,  $C_{p,a}$  is the specific heat of the air,  $C_{Ho}$  is the bare soil heat transfer coefficient, and  $v_a$  is the average wind velocity.

Precipitation Convection. The rain is handled separately with a simple advection formula given in Equation (38),

$$q_{Rain_k} = (T_{Rain} - T_k) \cdot A_k \cdot C_{Rain}. \quad (38)$$

$C_{Rain}$  is the rain convection conductor and is defined as

$$C_{Rain} = \rho \cdot v \cdot C_p = 1.1611 \cdot v. \quad (39)$$

The average rain velocity (mm/hr) is expressed as  $v$ ,  $\rho$  is the density of water, and  $C_p$  is the specific heat of water.

Ground Layer Conduction. Soil conductance is a function of the current moisture level and soil type. The conduction in the terrain nodes is only one dimensional through the layers and the elements do not transfer heat from neighboring transverse nodes.

$$q_{conduction_k} = (T_2 - T_k) \cdot A_k \cdot C_{kk_1} \quad (40)$$

$$C_{kk_1} = \frac{k(w_1)}{d_1} \quad (41)$$

In Equation (40),  $C_{kk_1}$  is the ground layer conduction and the thermal conductivity term,  $k$ , is a function of the soil moisture,  $w$ . The variable  $w_1$  is the volume fraction of surface soil moisture, and  $d_1$  is the surface layer thickness.

Solar Load.  $q_{netSolar_k}$  is the amount of incident solar energy absorbed by each node in Watts. This is a known quantity in the governing equation because it is not temperature dependent. The magnitude of incident solar energy is the combination of the following terms [ThermoAnalytics, 2000]

$$q_{netSolar_k} = q_{directSolar_k} + q_{reflected\_in\_solar_k} - q_{reflected\_out\_solar_k}, \quad (42)$$

where  $q_{directSolar_k}$  is the amount of incident solar energy absorbed from the measured direct solar irradiance (W),  $q_{reflected\_in\_solar_k}$  is the sum of the reflected energy from other

surfaces (W), and  $q_{reflected\_out\_solar_k}$  is the amount of energy not absorbed by the terrain elements, which is deflected to other enclosure elements (W).

The amount of incident solar energy absorbed from the measured direct solar irradiance,  $Q_{direct\_measured}$  (W/m<sup>2</sup>), is

$$q_{directSolar_k} = Q_{direct\_measured} \cdot \alpha_k \cdot A_{view_k}, \quad (43)$$

where  $\alpha_k$  is the absorptivity of the element  $k$  and  $A_{view_k}$  is the view area. The view area is the amount of the sun an element sees at a particular time and is defined as

$$A_{view_k} = A_{apparent_k} \cdot F_{visible_k}, \quad (44)$$

where  $F_{visible_k}$  is the visibility factor. The apparent area,  $A_{apparent_k}$ , defines the unshadowed area of the element projected in the direction of the sun. This projection also depends on the angle of incidence

$$A_{apparent_k} = (A_k) \cdot \cos(\beta), \quad (45)$$

where  $A_k$  is the area of element  $k$  and  $\beta$  is the angle of incidence. The visibility factor is the fraction of the element that is not shadowed (by other elements) when looking at it from the position of the sun. Clearly an element receives more energy when the incoming rays from the sun are not obstructed by another element. The visibility factor is calculated by ThermoAnalytics Ray Tracing algorithm at every time step. Rays are cast from different locations on the element towards the sun. The visibility factor determines the portion of an element that receives direct solar radiation. The Ray Trace algorithm will be discussed in greater detail in the next chapter. The angle of incidence,  $\beta$ , as

shown in Figure 15 is the angle between the element normal and the incoming ray from the sun.

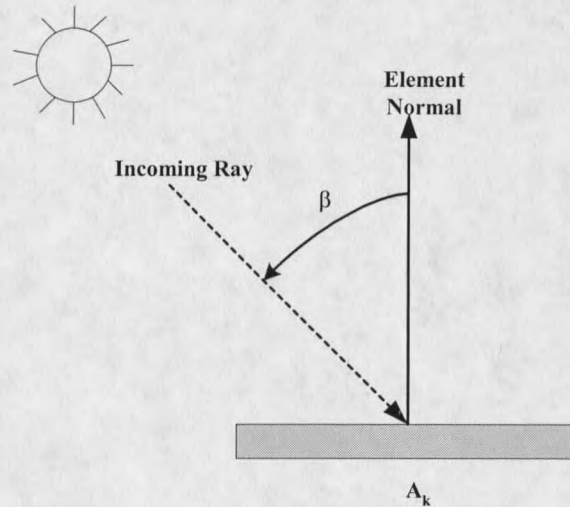


Figure 15. Angle of incidence.

The sum of the reflected energy is defined as

$$q_{reflected\_in\_solar_k} = q_{refl\_elements_k} + q_{diffuse\_in_k} + q_{refl\_default_k} \quad (46)$$

The  $q_{refl\_elements_k}$  term includes the incoming reflected solar radiation from other elements.

$q_{diffuse\_in_k}$  is the “first strike” diffuse solar irradiance (i.e. from the sky). This solar irradiance is not to be confused with the sky temperature, which is long wavelength radiation. Reflections from the default terrain onto the surface are accounted for in the term  $q_{refl\_default_k}$ . The default terrain is included in RadTherm/RT when an element sees beyond the portion of terrain that is explicitly modeled with specified terrain elements.

The amount of energy not absorbed by an element and reflected to other elements is represented by  $q_{reflected\_out\_solar_k}$ . Assuming that the terrain surfaces are gray and diffuse emitters, the amount of reflected radiation would be

$$q_{reflected\_out\_solar_k} = \left[ \begin{array}{l} Q_{direct\_measured} \cdot A_{view} + q_{relected\_in\_solar_k} \\ -(q_{directSolar_k} + q_{reflected\_in\_solar_k} \cdot \alpha_k) \end{array} \right] \quad (47)$$

The solution of  $q_{netSolar_k}$  is an iterative one. First, the sky assumed black and any solar radiation that is reflected back towards the sky does not get further reflected. An initial guess is made for  $q_{reflected\_out\_solar_k}$  for each node  $k$ . Then,  $q_{reflected\_in\_solar_k}$  is calculated for each node  $k$  (which depends on the guesses for  $q_{reflected\_out\_solar_k}$  for the other elements), and a better estimate for  $q_{reflected\_out\_solar_k}$  is calculated (i.e., it is just the reflected  $q_{reflected\_in\_solar_k}$ ). Then this process is repeated iteratively until the values for  $q_{reflected\_in\_solar_k} - q_{reflected\_out\_solar_k}$  converge to within some tolerance [Personal communication A. Curran].

Expanding Governing Equation. Expanding Equation (34) yields

$$CAP_{k_1} \cdot A_k \cdot \frac{\partial T}{\partial t} = \left[ \begin{array}{l} (T_a - T_k) \cdot A_k \cdot C_{ak} + (T_{k_2} - T_k) \cdot A_k \cdot C_{kk_1} + q_{radiation_k} + q_{netSolar_k} \\ +(T_{Rain} - T_k) \cdot A_k \cdot C_{Rain} \end{array} \right]. \quad (48)$$

For convenience, Equation (32) for the interior surface layers is repeated as

$$CAP_{k_i} \cdot A_k \cdot \frac{\partial T_{k_i}}{\partial t} = (T_{k_{i-1}} - T_{k_i}) \cdot A_k \cdot C_{kk_{i-1}} + (T_{k_{i+1}} - T_{k_i}) \cdot A_k \cdot C_{kk_i}. \quad (49)$$

The only unknowns in Equation (48) are  $q_{radiation_k}$ , the surface temperature  $T_k$ , and the interior layer temperature  $T_{k_2}$ . When Equation (49) is written for each of the interior nodes of each element it gives  $N_{Layers} - 1$  equations and  $N_{Layers}$  unknowns,  $T_k$  through  $T_{k_{N_{Layers}}}$ . Combining this with Equation (48) gives  $N_{Layers}$  equations and  $N + 1$  unknowns. The additional unknown is the  $q_{radiation_k}$  term. In order to solve this system of equations, the enclosure theory is introduced to solve for  $q_{radiation_k}$ .

Net-radiation Method – Enclosure Theory. The radiation term  $q_{radiation_k}$  in Equation (47) is solved using the Net-radiation Method Enclosure Theory. An enclosure is an area that is completely surrounded by solid surfaces or open areas. Thus an enclosure accounts for all directions surrounding the terrain by defining a volume that includes the terrain, background terrain, and sky dome. The radiation exchange between diffuse-gray surfaces in an enclosure is determined by the net-radiation equation of the Enclosure Theory. The net-radiation equation is in terms of node emissivity, surface area, the Stephan-Boltzmann constant, the view factor from node  $k$  to node  $j$ , and the temperatures of nodes  $k$  and  $j$  [ThermoAnalytics, 2000].

The enclosure is composed of  $N$  discrete surfaces (or elements), which are taken as both diffuse and gray. The term diffuse indicates that the directional emissivity and directional absorptivity do not depend on direction. Therefore, similar to a blackbody, the emitted intensity will be uniform over all directions. Spectral emissivity and spectral absorptivity of a gray surface are independent of wavelength but do depend on temperature. Due to this assumption, at each surface temperature the emitted radiation

will be the same fraction of blackbody radiation for all wavelengths [Siegel and Howell, 1981]. To summarize, a diffuse-gray surface absorbs a fixed fraction of incident radiation from any direction and at any wavelength and emits radiation that is a fixed fraction of blackbody radiation for all directions and wavelengths [Siegel and Howell, 1981]. Therefore, for a diffuse-gray surface in an enclosure, the total (hemispherical) emissivity of the surface is equal to its total (hemispherical) absorptivity [Incropera and DeWitt, 1996]. This relationship is known as Kirchoff's law,

$$\varepsilon = \alpha . \quad (50)$$

Another condition that must be met is each surface or element of the enclosure must be at a uniform temperature. As a result, the emitted energy is taken to be uniform over the surface of each element of the enclosure [Siegel and Howell, 1981].

Part of the energy incident on the surface is reflected. Because the surface have been defined as gray, the first assumption made for the reflected energy is that it is diffuse. This assumption indicates that the reflected intensity at each position is uniform for all directions. The second assumption is the reflected energy is uniform over each element of the enclosure. Therefore, the reflected and emitted energy for each surface have the same diffuse and equally distributed characteristics [Siegel and Howell, 1981].

Energy leaving a surface does not vary with angular direction if the surface is both a diffuse emitter and diffuse reflector. View factors can be introduced for a non-black surface if the diffuse-uniform condition applies to both the reflected and emitted energy.

The net-radiation method will be used to simplify the complex radiative exchange that occurs inside an enclosure. To derive the net-radiation enclosure equation consider

the  $k^{\text{th}}$  surface area,  $A_k$ , of an enclosure (Figure 16), where  $Q_{in_k}$  is the rate of incoming radiant energy per unit inside area (irradiation) and  $Q_{out_k}$  is the rate of outgoing radiant energy per unit inside area (radiosity).

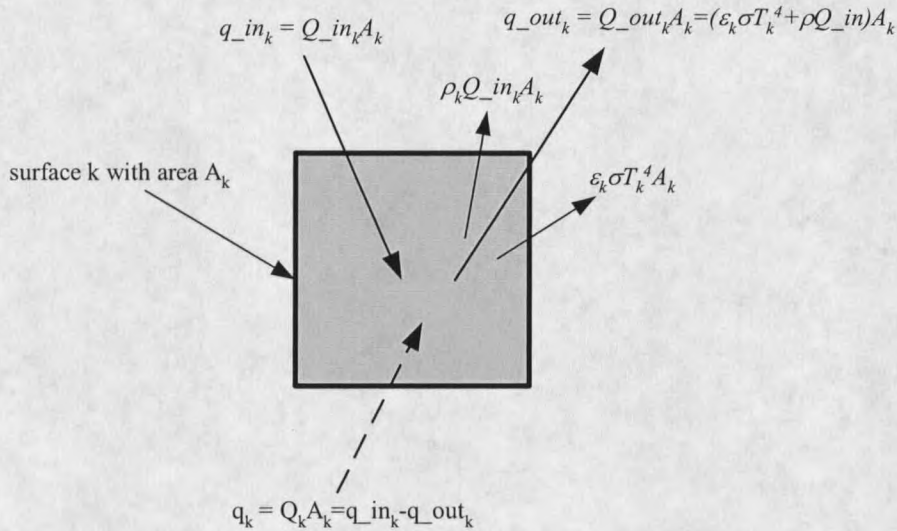


Figure 16. Energy quantities incident upon and leaving a typical surface of an enclosure.

$Q_k$  is the energy flux that would have to be transferred to the surface by another mode other than radiation to maintain the specified surface temperature [Incropera and DeWitt, 1996],

$$Q_k = Q_{out_k} - Q_{in_k}. \quad (51)$$

The net radiation heat transfer rate from surface  $k$  is

$$q_k = A_k \cdot (Q_{out_k} - Q_{in_k}). \quad (52)$$

Note that in general, the radiosity, or energy flux leaving the surface, is composed of directly emitted plus reflected energy. By definition,

$$Q_{out_k} = \varepsilon_k \cdot \sigma \cdot T_k^4 + \rho_k \cdot Q_{in_k}. \quad (53)$$

Reflectivity may be written using Equation (2) and Equation (50) as follows

$$\rho_k = (1 - \alpha_k) = (1 - \varepsilon_k). \quad (54)$$

Therefore, Equation (53) can be written as

$$Q_{out_k} = \varepsilon_k \cdot \sigma \cdot T_k^4 + (1 - \varepsilon_k) \cdot Q_{in_k}, \quad (55)$$

where the relations in Equation (54) are for opaque gray surfaces. Equations (52) and (53) are the basic equations for enclosure analysis. The key to simplifying the algebraic problem is to recognize that the irradiation in Equation (52) can be evaluated in terms of the radiosity of neighboring surfaces in the enclosure. If the  $k^{\text{th}}$  surface can view itself (i.e., it is concave), a part of its outgoing flux will contribute directly to its incident flux.

That is,

$$A_k \cdot Q_{in_k} = \sum_{j=1}^N F_{j-k} \cdot A_j \cdot Q_{out_j}. \quad (56)$$

Using the reciprocity property of view factors,

$$A_j \cdot F_{j-k} = A_k \cdot F_{k-j}, \quad (57)$$

Equation (56) can then be written alternatively as

$$A_k \cdot Q_{in_k} = A_k \cdot \sum_{j=1}^N F_{k-j} \cdot Q_{out_j}, \quad (58)$$

and reduces to

$$Q_{in_k} = \sum_{j=1}^N F_{k-j} \cdot Q_{out_j}. \quad (59)$$

Equations (55) and (59) provide two expressions for  $Q_{in_k}$ . Each of these equations is substituted into Equation (52) separately to get two basic heat balance equations for  $q_k$  in terms of  $Q_{out_k}$ . Solving Equation (55) for  $Q_{in_k}$  yields

$$Q_{in_k} = A_k \cdot \left( \frac{Q_{out_k}}{1 - \varepsilon_k} - \frac{\varepsilon_k \cdot \sigma \cdot T_k^4}{1 - \varepsilon_k} \right). \quad (60)$$

Substituting Equation (55) into Equation (52) yields

$$q_k = A_k \cdot \frac{\varepsilon_k}{(1 - \varepsilon_k)} \cdot (\sigma \cdot T_k^4 - Q_{out_k}). \quad (61)$$

Repeating the same process and substituting Equation (59) into Equation (52) gives

$$q_k = A_k \cdot (Q_{out_k} - \sum_{j=1}^N F_{k-j} \cdot Q_{out_j}). \quad (62)$$

The heat transfer rate for each element ( $q_k$ ) can then be defined as either the energy supplied to the surface  $k$  by nonradiative means (convection or conduction to  $A_k$ ), or as the net radiative loss from surface  $k$  resulting from radiation in the enclosure [Siegel and Howell, 1981]. Equations (61) and (62) represent the balance between the energy supplied by modes other than radiation and the net radiative loss.

In Equations (61) and Equation (62) the unknowns are  $q_k$ ,  $T_k$ , and  $Q_{out_k}$ . These equations can be written for each of the  $N$  surfaces in the enclosure. By combining these two equations,  $Q_{out_k}$  can be eliminated giving  $N$  equations relating the unknown  $q_k$ 's and  $T_k$ 's. To further explain this process, consider three surfaces in an enclosure. Using Equations (61) and (62), the pair of equations give

$$\frac{q_1}{A_1} = \frac{\varepsilon_1}{(1-\varepsilon_1)} \cdot (\sigma T_1^4 - Q_{-out_1}), \quad (63)$$

$$\frac{q_1}{A_1} = q_{o,k} - F_{1-1} \cdot Q_{-out_1} - F_{1-2} \cdot Q_{-out_2} - F_{1-3} \cdot Q_{-out_3}, \quad (64)$$

$$\frac{q_2}{A_2} = \frac{\varepsilon_2}{(1-\varepsilon_2)} \cdot (\sigma \cdot T_2^4 - Q_{-out_2}), \quad (65)$$

$$\frac{q_2}{A_2} = Q_{-out_2} - F_{2-1} \cdot q_{o,1} - F_{2-2} \cdot Q_{-out_2} - F_{2-3} \cdot Q_{-out_3}, \quad (66)$$

$$\frac{q_3}{A_3} = \frac{\varepsilon_3}{(1-\varepsilon_3)} \cdot (\sigma \cdot T_3^4 - Q_{-out_3}), \quad (67)$$

$$\frac{q_3}{A_3} = Q_{-out_3} - F_{3-1} \cdot Q_{-out_1} - F_{3-2} \cdot Q_{-out_2} - F_{3-3} \cdot Q_{-out_3}, \quad (68)$$

Equations (63), (65), and (67) are solved for  $Q_{-out_k}$  in terms of  $T_k$  and  $q_k$ . The resulting expressions for  $Q_{-out_k}$  are then substituted into equations (64), (66), and (68). This substitution eliminates the  $Q_{-out_k}$  terms and using summation notation, the resulting equations can be expressed as

$$\sum_{j=1}^N \left( \frac{\delta_{kj}}{\varepsilon_j} - F_{k-j} \cdot \frac{1-\varepsilon_j}{\varepsilon_j} \right) \cdot \frac{q_j}{A_j} = \sum_{j=1}^N (\delta_{kj} - F_{k-j}) \cdot \sigma \cdot T_j^4. \quad (69)$$

When writing Equation (69) for each surface,  $k$  takes on the values of  $1, 2, 3, \dots, N$ , and  $\delta_{kj}$  is the Kronecker delta defined as

$$\delta_{kj} = \begin{cases} 1 & \text{when } k = j, \\ 0 & \text{when } k \neq j. \end{cases} \quad (70)$$

In order to solve for  $q_k$ , Equation (69) can be expanded as

$$\begin{aligned} & \frac{-q_1}{A_1} \cdot F_{k-1} \cdot \frac{1-\varepsilon_1}{\varepsilon_1} - \frac{q_2}{A_2} \cdot F_{k-2} \cdot \frac{1-\varepsilon_2}{\varepsilon_2} - \dots + \frac{q_k}{A_k} \left( \frac{1}{\varepsilon_k} - F_{k-k} \frac{1-\varepsilon_k}{\varepsilon_k} \right) - \dots - \frac{q_N}{A_N} F_{k-N} \frac{1-\varepsilon_N}{\varepsilon_N} \\ & = -F_{k-1} \cdot \sigma \cdot T_1^4 - F_{k-2} \cdot \sigma \cdot T_2^4 - \dots + (1-F_{k-k}) \cdot \sigma \cdot T_k^4 - \dots - F_{k-N} \cdot \sigma \cdot T_N^4 \end{aligned} \quad (71)$$

Solving Equation (71) for  $q_k$  yields:

$$q_k = \frac{\varepsilon_k \cdot A_k}{1 - F_{k-k} \cdot (1 - \varepsilon_k)} \left[ \begin{aligned} & \sum_{j=1}^N \sigma \cdot F_{k-j} \cdot (T_k^4 - T_j^4) + \\ & \sum_{j=1}^N \left( (1 - \delta_{kj}) \cdot F_{k-j} \cdot \frac{1 - \varepsilon_j}{\varepsilon_j} \right) \cdot \frac{q_j}{A_j} \end{aligned} \right] \quad (72)$$

The term  $q_k$  is the net radiative loss from the  $k^{\text{th}}$  surface and is equal to  $-q_{\text{radiation}_k}$  in Equation (34). Replacing  $q_{\text{radiation}_k}$  with  $-q_k$  in Equation (48) and solving for  $q_k$  gives the following equation [Marttila, 1999]:

$$q_k = \left[ \begin{aligned} & -CAP_{k_i} \cdot A_k \cdot \frac{\partial T_k}{\partial t} + (T_a - T_k) \cdot A_k \cdot C_{ak} + (T_2 - T_k) \cdot A_k \cdot C_{kk} + q_{\text{netSolar}_k} \\ & + (T_{\text{Rain}} - T_k) \cdot A_k \cdot C_{\text{Rain}} \end{aligned} \right] \quad (73)$$

### Numerical Method of Solution

RadTherm solves the energy balance equation simultaneously for convection, conduction, and radiation. The time-averaging Crank-Nicholson implicit finite difference scheme is applied to the final governing Equations (32), (72), and (73) for the numerical solution. ThermoAnalytics utilizes the time-averaging Crank-Nicholson method because it is one of the most versatile numerical methods available and the method is unconditionally stable and second order accurate in time and space [Marttila, 1999]. The following section describes the development of the final governing equations for transient

analysis. The solution to the temperature distribution is then described. A majority of the mathematics for this section have been eliminated due to its complexity. The complete development of the numerical solution is shown in Marttila 1999.

### Transient Formulation

The  $T_k^4$  terms in Equation (72) are linearized to make the radiation term proportional to a temperature difference rather than to the difference between two temperatures to the fourth power [Incropera and DeWitt, 1996] as shown

$$(T_k^4 - T_j^4) = (T_k + T_j) \cdot (T_k^2 + T_j^2) \cdot (T_k - T_j) \quad (74)$$

The Crank-Nicholson implicit finite difference method is applied to Equation (72), the net-radiation equation, to yield an equation for the heating rate ( $q_k$ ) for each surface,

$$q_k = \frac{\varepsilon_k A_k}{1 - F_{k-k}(1 - \varepsilon_k)} \left[ \sum_{j=1}^N \sigma F_{k-j} (T_k^2 + T_j^2) (T_k + T_j) \left( \frac{T_k' + T_k}{2} - \frac{T_j' + T_j}{2} \right) + \sum_{j=1}^N \left( (1 - \delta_{kj}) F_{k-j} \frac{1 - \varepsilon_j}{\varepsilon_j} \right) \frac{q_j}{A_j} \right], \quad (75)$$

where  $T_k'$  and  $T_j'$  represent values from the current time step. The non-primed terms refer to values from the previous time step. Again, the Crank-Nicholson method is applied to Equation (32) and solving for  $T_{k_i}'$  yields an equation for the interior surface nodes:

$$T_{k_i}' = \frac{2 \cdot \frac{CAP_{k_i} \cdot A_k}{\Delta t} \cdot T_{k_i} + (T_{k_{i-1}}' + T_{k_{i-1}} - T_{k_i}) \cdot A_k \cdot C_{kk_{i-1}} + (T_{k_{i+1}}' + T_{k_{i+1}} - T_{k_i}) \cdot A_k \cdot C_{kk_i}}{2 \cdot \frac{CAP_{k_i} \cdot A_k}{\Delta t} + C_{kk_{i-1}} \cdot A_k + C_{kk_i} \cdot A_k} \quad (76)$$

Equation (76) is written for each interior node  $T'_{k_2}$  through  $T'_{k_{N_{Layers}}}$  associated with every surface element  $k$ . Once more, the Crank-Nicholson method is used on Equation (73) and yields an equation for the surface node  $k$ ,

$$q_k = \left\{ \begin{array}{l} -\frac{CAP_k \cdot A_k}{\Delta t} \cdot (T'_k - T_k) + \left[ \left( \frac{T'_a + T_a}{2} \right) - \left( \frac{T'_k + T_k}{2} \right) \right] \cdot A_k \cdot C_{ak} \\ + \left[ \left( \frac{T'_{k_2} + T_{k_2}}{2} \right) - \left( \frac{T'_k + T_k}{2} \right) \right] \cdot A_k \cdot C_{kk} \\ + \left[ \left( \frac{T'_{Rain} + T_{Rain}}{2} \right) - \left( \frac{T'_k + T_k}{2} \right) \right] \cdot A_k \cdot C_{Rain} + \frac{q'_{netSolar_k} + q_{netSolar_k}}{2} \end{array} \right\} \quad (77)$$

To eliminate the term  $q_k$ , Equation (75) and Equation (77) are combined

$$\left[ \begin{array}{l} -2 \cdot \frac{CAP_k \cdot A_k}{\Delta t} \cdot (T'_k - T_k) + (T'_a + T_a - T'_k - T_k) \cdot A_k \cdot C_{ak} + (T'_{2_k} + T_{2_k} - T'_k - T_k) \cdot A_k \cdot C_{kk} \\ + (T'_{Rain} + T_{Rain} - T'_k - T_k) \cdot A_k \cdot C_{Rain} + q'_{netSolar_k} + q_{netSolar_k} \end{array} \right] \quad (78)$$

$$= \frac{\varepsilon_k A_k}{1 - F_{k-k}(1 - \varepsilon_k)} \left[ \begin{array}{l} \sum_{j=1}^N \sigma F_{k-j} (T_k^2 + T_j^2) (T_k + T_j) (T'_k + T_k - T'_j - T_j) \\ + 2 \sum_{j=1}^N \left( (1 - \delta_{kj}) F_{k-j} \frac{1 - \varepsilon_j}{\varepsilon_j} \right) \frac{q'_j}{A_j} \end{array} \right]$$

For the surface layers, solving Equation (78) for  $T'_k$  yields

$$T'_k = \frac{\left[ 2 \cdot \frac{CAP_k \cdot A_k}{\Delta t} \cdot T_k + \frac{\varepsilon_k A_k}{1 - F_{k-k}(1 - \varepsilon_k)} \sum_{j=1}^N \sigma F_{k-j} (T_k^2 + T_j^2) (T_k + T_j) (T'_j + T_j - T_k) \right.}{\left[ 2 \cdot \frac{CAP_k \cdot A_k}{\Delta t} + \frac{\varepsilon_k A_k}{1 - F_{k-k}(1 - \varepsilon_k)} \sum_{j=1}^N \sigma F_{k-j} (T_k^2 + T_j^2) (T_k + T_j) + \right.}, \quad (79)$$

$$\left. + (T'_a + T_a - T_k) \cdot A_k \cdot C_{ak} + (T'_{k_2} + T_{k_2} - T_k) \cdot A_k \cdot C_{kk} + \right. \\ \left. (T'_{Rain} + T_{Rain} - T_{Rain}) \cdot A_k \cdot C_{Rain} + Q'_{netSolar_k} + Q_{netSolar_k} \right. \\ \left. - \frac{2\varepsilon_k A_k}{1 - F_{k-k}(1 - \varepsilon_k)} \sum_{j=1}^N \left( (1 - \delta_{kj}) F_{k-j} \frac{1 - \varepsilon_j}{\varepsilon_j} \right) \frac{q_j}{A_j} \right. \\ \left. C_{kk} \cdot A_k + C_{ak} \cdot A_k + C_{Rain} \cdot A_k \right]$$

which is the equation that is used in the numerical solution [Marttila, 1999].

### Computation of Temperature Distribution

To determine the temperature distribution through each element, the discretized governing Equations (79) and (76) are applied to each thermal node. This application results in  $N$  equations and  $2N$  unknowns for each  $T_k$  and  $q_{k_i}$  for all elements. For the initial time step the matrix is solved for steady state. A guess for  $T_k$  is made which leaves  $N$  equations and  $N$  unknowns. Gauss elimination with partial pivoting is used as a preconditioner to solve the resulting system of equations. The advantage of using Gauss elimination is the equations are solved simultaneously, which allows the node temperatures to converge quickly from initial values to the temperatures that satisfy the governing equations. After the direct solution (i.e. Gauss solution) is complete, the solution proceeds with an iterative method, Successive Overrelaxation (SOR). The governing Equations (75), (76), and (79) are evaluated for each node using the SOR iteration. SOR is a technique that can be used to accelerate any iterative procedure by

making corrections to particular values before the next iteration [Tannehill et al, 1997]. Once all node temperatures have converged, the iteration is complete. The solution then advances to the next time step and repeats the above procedure [Marttila, 1999].

## CHAPTER 3

## METHODOLOGY

One of the main factors that determine the radiation exchange between surfaces is the view factor. A view factor is defined as the fraction of radiation leaving a surface  $x$ , which is then intercepted by surface  $y$ . The view factor depends on three main factors: size of surface, shape of surface, and orientation of surface. ThermoAnalytics has developed a ray-tracing algorithm that computes the view factors for each element and is discussed in the following section.

In this chapter a simple model is introduced to explain the motivation for deleting elements by the use of view factors. The effects of shading and a look at longwave and shortwave radiation exchange between surfaces is investigated. By using simple models these areas are explored and the use of view factors is discussed. The last part of the chapter describes the analytical approach used to delete elements by the use of view factors.

Ray-Tracing Algorithm

Radiation view factors are used in ThermoAnalytics' software to model the radiation heat rate from each element to every other element in the model and to the environment [ThermoAnalytics, 2000]. This allows the terrain model to include the full effects of solar shadowing, multiple reflections, and re-radiation of geometric features. Each triangular surface element (or facet) of the terrain has a view factor to the background,

sky, and other elements [www.thermoanalytics.com]. Note that each element's surface is planar. ThermoAnalytics computes both radiation view factors and solar projected (apparent) areas by the use of a ray tracing algorithm which casts rays from each element.

The geometric view factors are calculated initially at the start of a RadTherm/RT run using the ray trace technique. This is done first and only once for a given terrain model. These view factors are based only on the geometry of the terrain file and are calculated prior to the thermal solution. A view factor file (.vfs) is created, which is then used for the calculation of the thermal solution.

The ray trace algorithm is then used during the thermal solution, at each time step, to calculate the view area for each surface element (Equation(44)). Rays are cast from the centroid of each element to the sun, which accounts for the amount of direct solar radiation that reaches each surface element. At the specified geographic location and time, the positions of the primary source of irradiation (the sun) is defined by two angles, the solar azimuth and zenith angles, that are updated at each time step. The angle from the vertical is the zenith angle, and the angle measured counter-clockwise in the horizontal plane from the reference direction is the azimuth angle as shown in Figure 17.

To better explain the ray tracing technique consider two parallel plates (Figure 18a). A unit hemisphere is created at the centroid of each element. Figure 18a illustrates a single ray being cast and intercepted by another element.

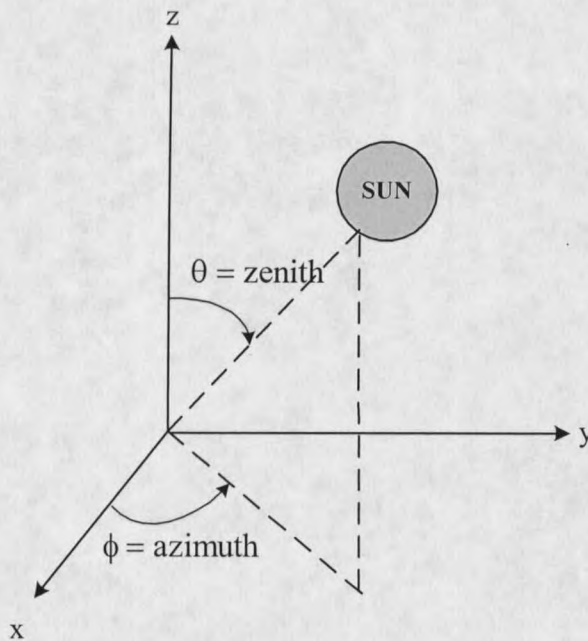
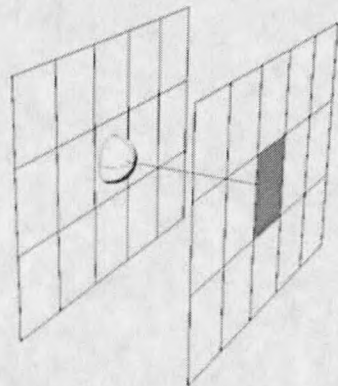


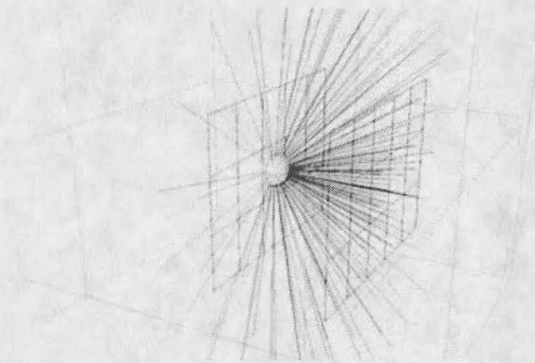
Figure 17. The position of the sun is specified in terms of the zenith and azimuth angles,  $\theta$  and  $\phi$ , respectively.

A set number of rays, chosen by the user, are cast from each element centroid to determine the view factor to many of the other elements that are visible from the element centroid. The hemisphere is then equally subdivided based on the number of rays to be cast. These subdivisions are a function of the angle  $\theta_i$ , which is defined so the population of rays cast will be the greatest near the element normal [www.thermoanalytics.com]. The number of rays that intersect another element determines the strength or weight of the view factor. Figure 18b shows multiple rays cast from an element by the use of the ray trace algorithm to determine its view factor relationships to all other elements in the enclosure.



ThermoAnalytics, Inc.

(a)



ThermoAnalytics, Inc.

(b)

Figure 18. (a) A single ray cast from an element for ThermoAnalytics Ray Trace Algorithm. (b) Multiple rays cast from an element for ThermoAnalytics Ray Trace Algorithm. (Figures from ThermoAnalytics, Inc. website)

### View Factor Rays

The number of rays cast from the element centroid is determined by the user-assigned “View Factor Rays”. By adjusting the number of rays cast from each element, the speed and accuracy of the view factor calculation is determined. Five different settings are available in RadTherm. Selecting setting 1 cast 512 rays from each element. This gives the fastest solution time with the least amount of accuracy. Setting 5 cast 4608 rays from each element which gives the most accurate solution but the computation time is much slower. [ThermoAnalytics, 1999]. Table 1 shows the different settings for the view factor rays.

Table 1. View factor ray setting in RadTherm/RT.

Setting	Rays Cast from each Element
1	512 (fastest)
2	1152 (default)
3	2048
4	3200
5	4608 (most accurate)

### View Factor Subdivisions

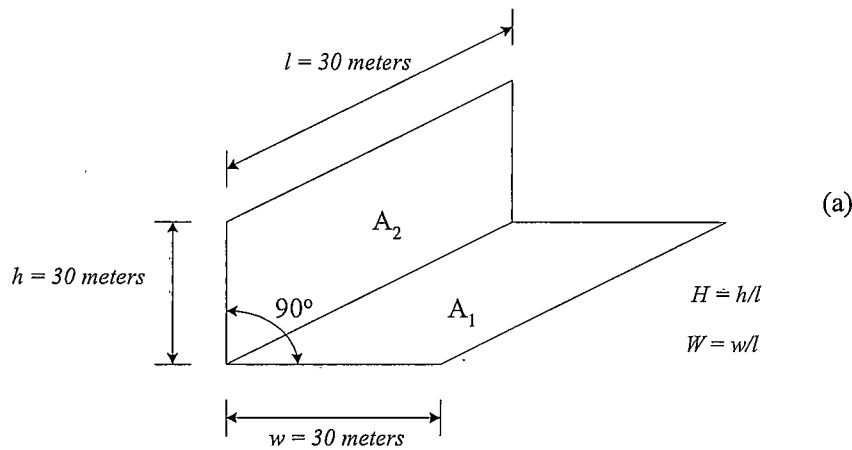
Another user-defined setting is the number of subdivisions per element. Each element has one to five subdivisions and rays are cast from the centroid of each subdivision. The amount of subdivisions increase the number of rays cast from each element from one to five times the view factor ray setting. As the number of subdivisions increase, the thermal run time and view factor calculations can increase significantly [ThermoAnalytics, 1999].

### Apparent Area Resolution

Apparent Area Resolution changes the number of rays that are cast from the centroid of each element to the sun used for calculating apparent area. At the lowest setting only a single ray is cast from the centroid of each element to the sun and at the highest setting 64 rays are cast.

### Hand Calculation for View Factor

A simple model is used to compare the results of the view factor using the ray trace algorithm and a hand calculation for the view factor. Figure 19a illustrates the simple model that consists of two 30-meter by 30-meter rectangles at an angle of ninety degrees to each other.



$$F_{1-2} = \frac{1}{\pi \cdot W} \left( W \cdot \tan^{-1} \frac{1}{W} + H \cdot \tan^{-1} \frac{1}{H} - \sqrt{H^2 + W^2} \cdot \tan^{-1} \frac{1}{\sqrt{H^2 + W^2}} + \frac{1}{4} \cdot \ln \left\{ \frac{(1+W^2)(1+H^2)}{1+W^2+H^2} \left[ \frac{W^2(1+W^2+H^2)}{(1+W^2)(W^2+H^2)} \right]^{W^2} \left[ \frac{H^2(1+H^2+W^2)}{(1+H^2)(H^2+W^2)} \right]^{H^2} \right\} \right) = 0.20 \quad (b)$$

Figure 19. (a) A simple model used for the hand calculation of the view factor. The model consists of two finite rectangles of the same length, having one common edge at an angle of  $90^\circ$  to each other. (b) The equation used to calculate the view factor from 1 to 2. (After Siegel and Howell, Figure 16 in the Appendix)

The equation in Figure 19b was used to calculate the view factor from 1 to 2. The result using the equation is  $F_{1-2} = 0.20$ . The identical model in Figure 19a was created in

RadTherm/RT consisting of two elements,  $A_1$  and  $A_2$ . The view factors calculated for elements 1 and 2 using the ray trace algorithm are shown in Table 2. Element 3 is the default terrain node and element 4 is the sky node.

Table 2. View factor ray setting in RadTherm/RT.

Emitter #	Receiver #	View Factor
1	2	0.1913
1	4 (Sky node)	0.8087
<b>View factor sum:</b>		<b>1.00</b>

Emitter #	Receiver #	View Factor
2	1	0.1913
2	3 (Default terrain node)	0.3089
2	4 (Sky node)	0.4998
<b>View factor sum:</b>		<b>1.00</b>

The hand calculation for the view factor was 0.20 and the value computed using the ray trace algorithm was 0.1913. The ray trace algorithm provides similar results to the hand calculation for the view factor.

### The Process to Delete Elements

The motivation for this thesis came from the initial results of the previous section. Basic models were created to determine the importance of the radiation exchange between surfaces. The results prompted the idea that view factors could be used to eliminate elements that have no influence on the temperature of an area of interest. Recall there is a limitation on the size of the thermal map for which RadTherm/RT can compute the thermal solution. If a methodology is created to reduce the number of elements in a thermal map for RadTherm/RT, larger regions of interest can be modeled in

the software. Therefore, the task was to determine a computational approach for reducing the number of elements in the map without losing accuracy or significantly reducing the region of interest. Currently, Bozeman Pass is being used as a test bed for traveler or maintenance weather information. This is the primary region of focus for this thesis and the goal is to increase the length of the highway that can be modeled and/or speed runtime of forecast models.

The current map used for Bozeman Pass was first trimmed down and then remeshed with increasing element size as distance from the interstate increased. Based only on intuition using a topographic map, there is no precise approach for reducing the modeled area. The user must estimate using important ridgelines and create boundaries based on the assumption that the remaining terrain is significant for the thermal solution, and terrain removed was not. A second source of inaccuracy is the process by which the map is remeshed. The procedure for this is to keep the original dimension of the map and combine elements that are further away from the elements of interest, i.e., the highway. This is a misrepresentation of the elements because it involves combining elements of different terrain types, such as water, trees, rock, soil, etc. In addition to these downfalls, it can be a time-consuming and labor-intensive process to generate the coarsened map.

An alternative approach that is more efficient and more accurate is presented here. In order to complete this task, the number of surface elements in the map will be reduced by eliminating elements using the view factor information relating each element to all other elements. The main objective is to ensure that the removed elements do not include

terrain that is pertinent to the temperature of the highway. In the following section, the procedure used to delete the elements is discussed.

### Initial Setup

In order to create a thermal model in RadTherm/RT for a particular region of interest, two files are required. The first file contains Digital Elevation Map (DEM) data, and the other provides land cover data used to identify vegetation and road positions in the model. The information is provided in ASCII format and used to create the maps for RadTherm/RT. Montana State University's Geographic Information and Analysis Center (GIAC) produced the ASCII files for elevation, road and vegetation maps using ARC/INFO geographic information system (GIS) software [Adams and Curran, 1999].

#### Step 1a - Digital Elevation Map Files (.asc)

Elevation data was compiled from a United States Geological Survey (USGS) 30-meter DEM. Digital Elevation Model (DEM) is the terminology adopted by the USGS to describe data sets in a digital raster form. The standard DEM consists of a regular array of elevations cast on a designated coordinate projection system. The orientation of data is by columns and rows. Each column contains a series of elevations ordered from north to south with the order of the columns from west to east. These data were collected as part of the National Mapping Program. The entire set of data was then projected on the Universal Transverse Mercator (UTM) coordinate system. The grids are then exported as ASCII files. An example data file is shown in Figure 20.

```

DEM File - WordPad
File Edit View Insert Format Help
[Icons]
ncols      357
nrows     189
xllcorner 511313.156
yllcorner 5053505.5
cellsize  30
NODATA_value -9999
1722.057 1720.041 1718.978 1719.937 1720.
1710.142 1706.047 1705.091 1700.191 1696.
1722.063 1720.069 1718.029 1717.966 1718.
1701.019 1701.119 1698.165 1697.085 1697.
1721.023 1720.046 1718.047 1717.006 1716.
1709.05  1710.098 1709.152 1708.156 1707.
1720.023 1719.04  1717.041 1716.011 1715.
1721.213 1719.18  1719.115 1719.102 1720.
1719      1718.035 1716.018 1715.971 1716.
1732.167 1731.072 1732.056 1732.078 1732.
1716.995 1716.03  1714.013 1713.955 1714.
1742.256 1735.256 1732.025 1733.918 1733.
1715.018 1714.03  1712.03  1710.99 1710.5
1732.082 1731.113 1727.048 1727.923 1727.
For Help, press F1
NUM

```

Figure 20. Example of ASCII input file for elevation data created from USGS 30 meter grid.

Header information is included at the top of the file, containing the number of rows and columns, the x-y origin of the lower left corner of the grid, the cell size, and the value used for “no data” in the grid. The 357 x 189 grid for this map in Figure 20 represents a 10680-meter x 5640-meter terrain map.

#### Step 1b - Terrain File (.asc)

The vegetation information was a product of the Montana Gap Analysis project (MT-GAP). This project created a classification system for existing vegetation in Montana. Part of this classification system is shown in Table 3.

Table 3. Land cover classification system used by Montana Gap Analysis Project.

Land Cover Class Code	Land Cover Class
2010	Agricultural Lands - Dry
2020	Agricultural Lands - Irrigated
3110	Altered Herbaceous
3130	Very Low Cover Grasslands
3150	Low/Moderate Cover Grasslands
3170	Moderate/High Cover Grasslands
3180	Montana Parklands and Subalpine Meadows
3210	Mixed Mesic Shrubs
3300	Mixed Xeric Shrubs
3310	Salt-Desert Shrub/Dry Salt Flats
3350	Sagebrush
3510	Mesic Shrub-Grassland Associations
3520	Xeric Shrub-Grassland Associations
4000	Low Density Xeric Forest
4140	Mixed Broadleaf Forest
4203	Lodgepole Pine
4205	Limber Pine
4206	Ponderosa Pine
4212	Douglas-fir
4214	Rocky Mountain Juniper
4223	Douglas-fir/Lodgepole Pine
4260	Mixed Whitebark Pine Forest
4270	Mixed Subalpine Forest
4290	Mixed Xeric Forest
4300	Mixed Broadleaf and Conifer Forest
6110	Conifer Riparian
6120	Broadleaf Riparian
6130	Mixed Broadleaf and Conifer Riparian
6200	Graminoid and Forb Riparian
6300	Shrub Riparian
6400	Mixed Riparian
7300	Rock

Montana State University's Geographic Information and Analysis Center (GIAC) produced an ASCII file for vegetation using ARC/INFO software, which is a GIS software program. The data set is an ARC/INFO 90 meter land cover grid (raster file) covering the state of Montana. A raster file contains information that is directly mapped



## Step 2 - Trimming the Original Map

The main objective is to delete unnecessary elements from a map using the view factor information of each highway element. This information is found in the view factor file (.vfs) initially generated at the start of a run in RadTherm/RT. Once a RadTherm/RT project is created, the model is executed and the first item produced is the view factor file. The software continues to run and the final result is the thermal solution to the terrain map. If a RadTherm/RT project is too large, a limited amount of disk space or computer memory may cause the project to fail. There are two possible outcomes if the RadTherm/RT project contains too many elements. First, the computer can crash and neither the view factor file nor the thermal solution will be completed. Second, the view factor file can complete successfully and then the computer stalls and terminates on the thermal solution. Therefore, RadTherm/RT may produce the view factor file even when the thermal solution cannot be solved. As a result, the largest number of surface elements that can produce the view factor file must be determined. The view factor file is explained in more detail later in this chapter.

A map of Bozeman Pass with dimensions of 16.09 by 27.36 kilometers was used as a starting point to create the view factor file. This map contained 831,174 surface elements and was too large to process even the view factor file. By using a PERL script the map can be cropped by specifying the north, east, south and west UTM coordinates [McKittrick, personal communications]. The command line to execute the script is shown in Figure 22. Note that the script uses both the vegetation and elevation files.

```
$ gis_manip -S[UTM coord] -N[UTM coord] -E[UTM coord] -W[UTM coord] [filename]
```

Note: filename is without \_dem.asc or \_veg.asc extension

Figure 22. Command line to execute the gis\_manip PERL script.

As an example, the first iteration reduces the map to a size of 8.05 by 27.36 kilometers and contains 544,810 surface elements. After over three hours of computation time, the view factor file was only 7% complete. Based on experience, at this point the run was killed, realizing that it would never reach completion. For the next iteration, the map was cut down to 387,340 surface elements. The view factor file after seven hours of run time was only 27% complete and once again the view factor file could not be generated. The final iteration left a map with 327,610 surface elements. A project of this size produced a completed view factor file after almost sixteen hours but crashed on the thermal solution. This was used as the target number of elements to begin the process of deleting surface elements. Table 4 summarizes the findings of this iterative process.

Table 4. Summary of the iterations for trimming a map of Bozeman Pass to a size that produces the view factor file (.vfs).

	# Elements	View Factor File
<b>Original Map</b>	831,174	Failed
<b>Iteration #1</b>	544,810	Failed
<b>Iteration #2</b>	387,340	Failed
<b>Final Iterations</b>	327,610	Complete

There are several items that must be set in RadTherm/RT once a project has been created with less than 330,000 surface elements. First, an appropriate weather file is selected, and then the same start and end times are set on the GUI. This ensures the thermal solution is not calculated, but the view factor file is still generated. Each part in the project is set to type terrain but no other information has to be specified. Figure 23 shows the steps described above.

Finally, the RadTherm/RT project is executed and the view factor file is created. This information is only geometry dependent and therefore does not change at every time step. The file is created once and can be used in successive runs as long as the geometry of the map does not change. Figure 24 highlights the steps of the process to this point.

### Step 3 - RadTherm/RT Project Files (.tdf)

Once a project is created in RadTherm, the file is saved as a .tdf file. The .tdf file is the native RadTherm file format, which stores both the geometry for the thermal model and the thermal analysis results. The RadTherm file is a binary file format that is platform independent, so that files written on one machine can be easily read on another machine that uses a different operating system.

In this case, a RadTherm project is created using the ASCII formatted vegetation and elevation file, filename\_dem.asc and filename\_veg.asc, respectively. First, the "File-open" command on the Graphical User Interface (GUI) prompts the user for the DEM and vegetation file.

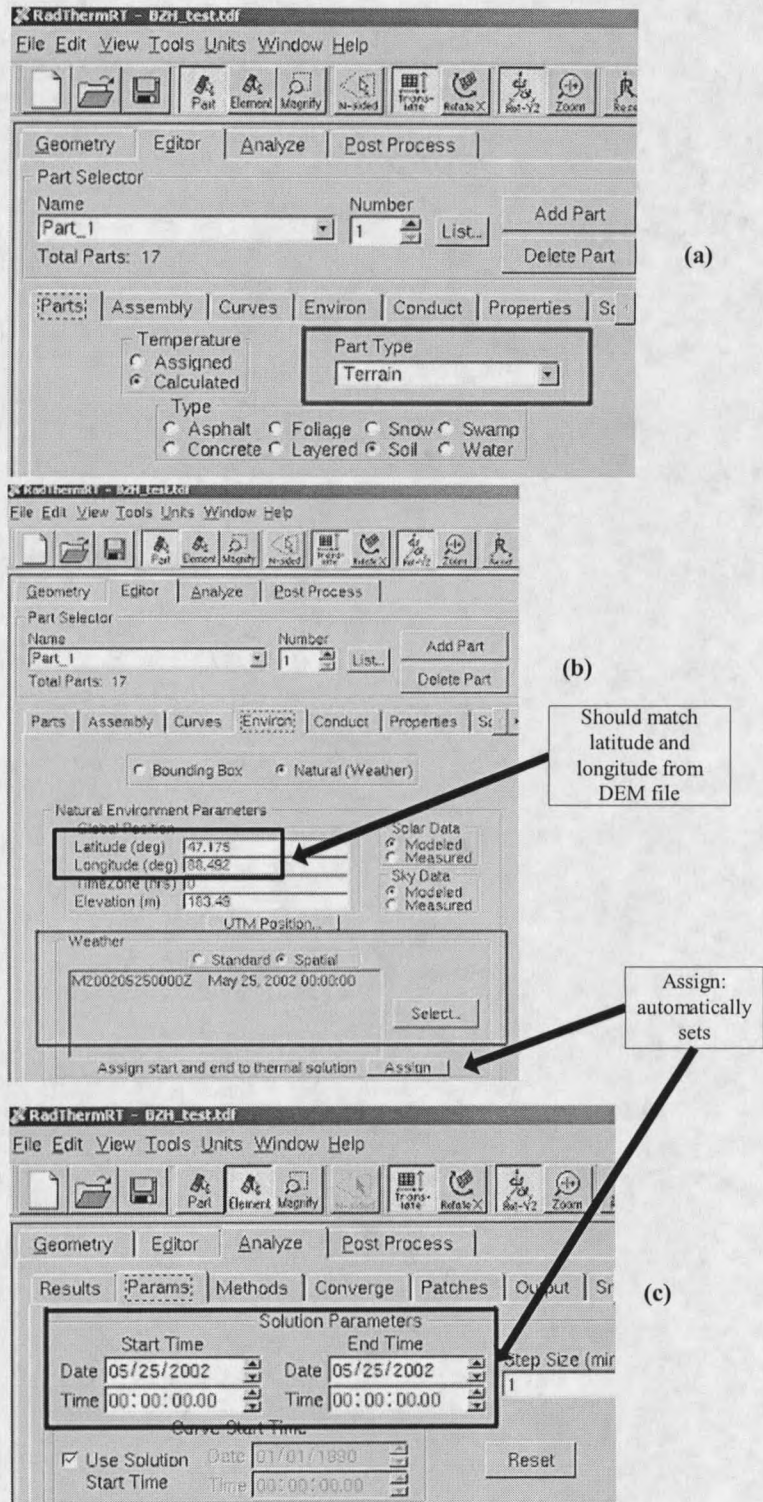


Figure 23. (a) Set each part to type terrain. (b) Specify a weather file. (c) Set the same start and end solution times.

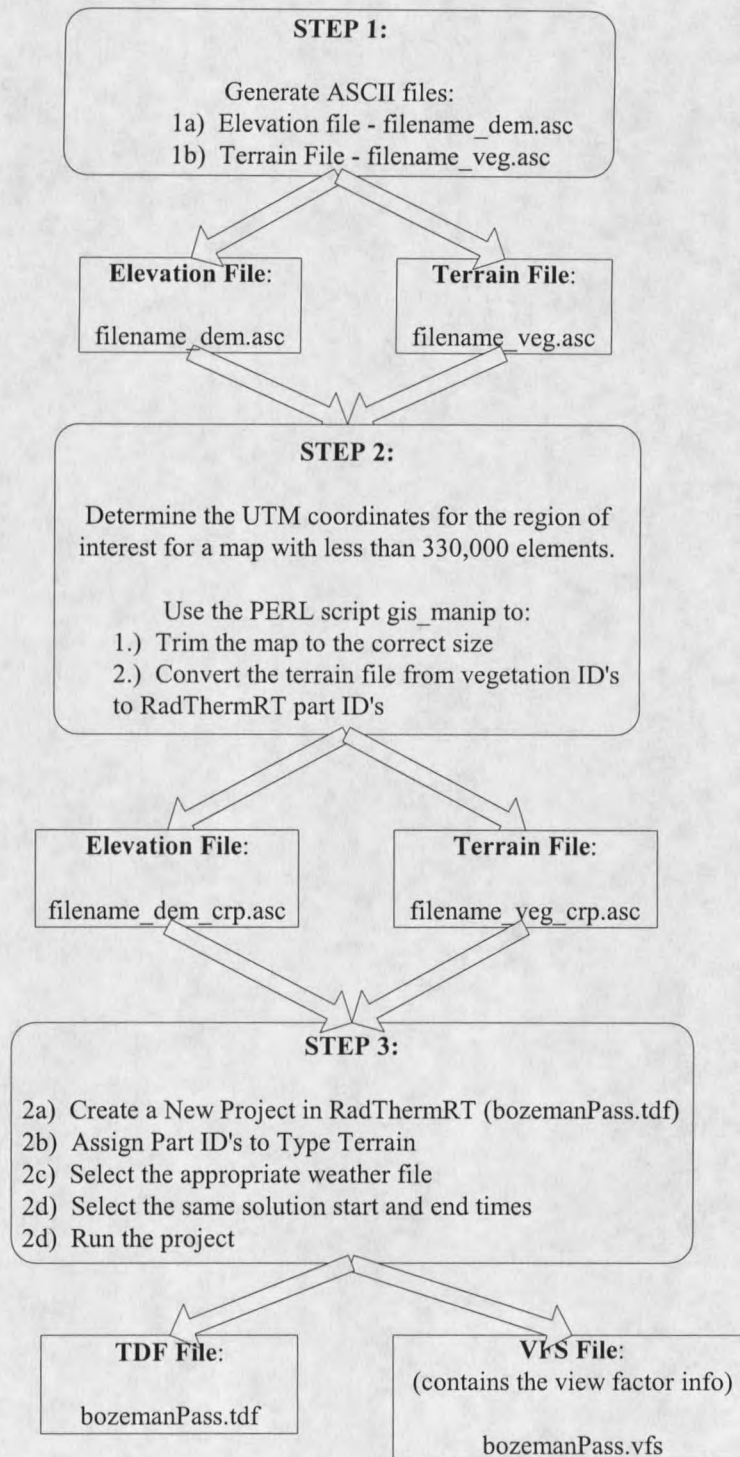


Figure 24. Flow chart of Steps 1 through 3. Step 1 is generating the ASCII files. Step 2 determines the UTM coordinates for a map with less than 330,000 elements. Step 3 creates a new project in RadTherm/RT.























































































































































































































































